The Fundamental Plane of Gravitational Lens Galaxies
and
The Evolution of Early-Type Galaxies in Low Density Environments [1]

C.S. Kochanek[a],

E.E. Falco[a], C.D. Impey[b], J. Lehár[a], B.A. McLeod[a]

H.-W. Rix[c], C.R. Keeton[b], J.A. Muñoz[a] and C.Y. Peng[b]

[a] Harvard-Smithsonian Center for Astrophysics, 60 Garden St., Cambridge, MA 02138
email: ckochanek, efalco, jlehar, bmcleod, jmunoz@cfa.harvard.edu
[b]Steward Observatory, University of Arizona, Tucson, AZ 85721
email: impey, ckeeton, cyp@as.arizona.edu
[c]Max-Planck-Institut fuer Astronomie, Koenigsstuhl 17, D-69117 Heidelberg, Germany
email: rix@mpia-hd.mpg.de

ABSTRACT

Most gravitational lenses are early-type galaxies in relatively low density environments – a "field" rather than a "cluster" population. Their average properties are the *mass-averaged* properties of all early-type galaxies. We show that field early-type galaxies with $0 < z < 1$, as represented by the lens galaxies, lie on the same fundamental plane as those in rich clusters at similar redshifts. We then use the fundamental plane to measure the combined evolutionary and K-corrections for early-type galaxies in the V, I and H bands. Only for passively evolving stellar populations formed at $z_f \gtrsim 2$ ($H_0 = 65$ km s^{-1} Mpc^{-1}, $\Omega_0 = 0.3$, $\lambda_0 = 0.7$) can the lens galaxies be matched to the local fundamental plane. The high formation epoch and the lack of significant differences between the field and cluster populations contradict many current models of the formation history of early-type galaxies. Lens galaxy colors and the fundamental plane provide good photometric redshift estimates with an empirical accuracy of $\langle z_{FP} - z_l \rangle = -0.04 \pm 0.09$ for the 20 lenses with known redshifts. A mass model dominated by dark matter is more consistent with the data than either an isotropic or radially anisotropic constant M/L mass model, and a radially anisotropic model is better than an isotropic model.

Subject headings: gravitational lensing: cosmology – galaxies: evolution – galaxies: photometry

---

[1]Based on Observations made with the NASA/ESA Hubble Space Telescope, obtained at the Space Telescope Science Institute, which is operated by AURA, Inc., under NASA contract NAS 5-26555.

1. Introduction

The formation and evolution of galaxies is a central problem of modern astronomy. In particular, observations show that most early-type galaxies in rich clusters formed their stars at an early epoch ($z_f \sim 2$–3) and have only evolved passively during the following 10 Gyr (e.g. Bower, Lucey & Ellis 1992). The early-type galaxies in clusters have extraordinarily uniform colors both internally and among clusters, as well as very tight correlations between color and velocity dispersion that are difficult to reconcile with a wide range of ages for their stellar populations. The uniformity of the colors persists to $z \sim 1$ (Ellis et al. 1997, Stanford, Eisenhardt & Dickinson 1998, Pahre 1999), although there is evidence that the S0 galaxies are evolving faster than the ellipticals (van Dokkum et al. 1998b). The fundamental plane or FP (Djorgovski & Davis 1987, Dressler et al. 1987), a tight correlation between effective radius, surface brightness and velocity dispersion for early-type galaxies, provides a powerful tool for probing their evolution. Local measurements of the FP at a range of wavelengths (e.g. Jorgensen, Franx & Kjaergaard 1995ab, 1996, Pahre, de Carvalho & Djorgovski 1998a) can be combined with measurements of the FP in rich clusters at intermediate redshifts (van Dokkum & Franx 1996, Kelson et al. 1997, 2000, van Dokkum et al. 1998a, Pahre, Djorgovski & de Carvalho 1999ab, Jorgensen et al. 1999) to directly measure the evolution of the mass-to-light ratio of early-type galaxies with cosmic epoch. This evolution is consistent with an early formation epoch for the stellar populations, and the FP results probably rule out, at least for cluster galaxies, the broad range of formation epochs inferred from modeling the line strengths of local early-type galaxies (e.g. Trager 1997, Jorgensen 1999, Terlevich et al. 1999, see Pahre, de Carvalho & Djorgovski 1998b).

Far less is known about the homogeneity and evolution of early-type galaxies in less dense environments than the cores of rich clusters, even though these galaxies represent the vast majority of the early-type galaxies. Semi-analytic models of galaxy formation, particularly those of Kauffmann (1996) and Kauffmann & Charlot (1998), predict that field early-type galaxies have very late forming stellar populations ($z_f < 1$), while cluster early-types have significantly older populations. In their models, however, the halos they identify as early-type galaxies appear to have old stellar populations at all epochs because the models also predict a rapidly evolving number density of early-type galaxies. The preponderance of the observational evidence suggests, however, that there is little evolution in the number of massive early-type galaxies to $z \simeq 1$ (Lilly et al. 1995, Schade et al. 1999), although contrary views exist (Kauffmann, Charlot & White 1996). If the number density evolves little, then the early-type galaxies near $z = 1$ must be the precursors of those at $z = 0$. Studies of local early-type galaxies find some evidence that field early-type galaxies have younger stellar populations (e.g. de Carvalho & Djorgovski 1992, Guzmán & Lacey 1993, Forbes, Ponman & Brown 1998, James & Mobasher 1999), but with similar difficulties untangling age from metallicity as are found in the cluster samples. As with the cluster galaxies, the best way to separate age from metallicity is to look at earlier epochs. Schade et al. (1996, 1999) have used the correlation between effective radius and luminosity to show that the luminosity evolution of field and cluster early-type galaxies is similar at $z \sim 0.5$. Treu et al. (1999) constructed the fundamental plane of six field early-types near $z = 0.3$ and found that it was consistent with that found by van Dokkum & Franx (1996) and Kelson et al. (1997) for the cluster sample. The absence of extremely red galaxies in deep surveys sets a weak upper bound on the star formation epoch of $z_f \lesssim 5$ (e.g. Zepf 1997). It is a weak upper bound because a

very small amount of late-time star formation will make a galaxy bluer than the extreme colors $(V - K > 7 \text{ mag})$ used to obtain the limit.

The population of gravitational lens galaxies is dominated by massive early-type galaxies (Keeton, Kochanek & Falco 1998), as expected from theoretical predictions (e.g. Fukugita & Turner 1991, Maoz & Rix 1993, Kochanek 1993, 1996). The lens galaxies are selected based on their mass rather than on any property related to star formation,[2] leading to a sample dominated by L_* early-type galaxies. Indeed, since the lensing cross section is closely related to the mass of the lens, the average properties of the lens galaxies at any redshift are nearly identical to the *mass-weighted* average properties of all galaxies at that redshift. The lens galaxies are also a "fair" sample of the environmental distribution of early-type galaxies. The exception is that galaxy-dominated lenses will not be found in the cores of rich clusters where the cluster potential dominates any lensing effects and produces phenomenon such as giant arcs rather than the lenses we discuss here. Thus, we will refer to the lenses as a sample of "field" early-type galaxies or early-type galaxies in "low-density" environments, as very few lie in group or cluster potentials with velocity dispersions larger than the 400 km s^{-1} break used by Kauffmann & Charlot (1998) to divide early-type galaxies into field and cluster samples. Keeton et al. (1998) estimated the evolution of the mass-to-light ratio of the lens galaxies with redshift, and found rates strikingly similar to those measured for the rich cluster samples.

The CASTLES (CfA-Arizona Space Telescope Lens Survey) survey is obtaining V, I and H photometry of the 60 known lens systems. Since the geometry of a gravitational lens provides an accurate measurement of the lens galaxy's mass, the lens galaxies are one of the largest samples of galaxies with accurately measured masses at intermediate redshifts, and they are by far the largest such sample outside the very special environments represented by the cores of rich clusters. In §2 we describe our analysis methods and the data. In §3 we compare the colors of the lens galaxies to those of the rich cluster galaxies used in the FP studies at intermediate redshift. In §4 we show that the lens galaxies lie on the same FP as the cluster galaxies at comparable redshifts. In §5 we explore photometric redshift estimates for the lens galaxies, and in §6 we explore the dark matter problem in early-type galaxies. In §7 we use the FP to measure the evolution of early-type galaxies in the V, I and H bands as a function of redshift. Finally, in §8 we summarize our results.

2. Methods and Models

In this section we detail our local comparison sample (§2.1) and our method for using the FP to study the evolution of individual galaxies (§2.2). Next we discuss how we estimate stellar velocity dispersions from the lensed image separations in several dynamical models (§2.3) and the available sample of gravitational lens galaxies (§2.4). Finally, we discuss the interpretation of the results using either spectrophotometric models (§2.5) or comparisons to early-type galaxies in

---

[2]The optically selected lenses are biased against star forming lens galaxies to the extent that any associated dust obscures background sources (see Falco et al. 1999). Because almost all optically-selected lenses are very bright quasars, the lower mass-to-light ratios of star forming galaxies do not produce a bias (see Kochanek 1996). Radio selected lenses are immune to both effects.

clusters at comparable redshifts (§2.6).

2.1. The Local FP

Unlike the studies of the FP in rich clusters, we must work with individual galaxies spread over a wide range of redshifts. Thus our analysis methods must be designed to interpret the data on individual galaxies rather than ensembles of galaxies at a common redshift. We use the early-type galaxies in nine local clusters studied by Jorgensen & Franx (1994) and Jorgensen, Franx & Kjaergaard (1995ab, 1996, collectively referred to as JFK hereafter) as a local comparison sample. We arbitrarily renormalized the JFK FP to the closest standard HST filter, F606W, from Gunn r assuming a constant color of $F606W - r = -0.09$ mag for early-type galaxies (Fukugita, Shimasaku & Ichikawa 1995). We also converted from the angular effective radius of the galaxies at the redshift of Coma ($cz \equiv 7200$ km s^{-1}) to a physical effective radius for $H_0 = 50h_{50}$ km s^{-1} Mpc^{-1}. We then redetermined the zero points of the FP relations holding the slopes fixed to the JFK values. For example, the physical effective radius r_e^{FP} predicted by the fundamental plane from the central velocity dispersion and the surface brightness of the galaxy is

$$\log\left(\frac{r_e^{FP}}{h_{50}^{-1}\text{kpc}}\right) = 1.24\log\left(\frac{\sigma_c}{\text{km s}^{-1}}\right) + 0.33\left(\frac{\mu_e(0)}{\text{mag/arcsec}^2}\right) - 8.66, \tag{1}$$

with a dispersion of 0.07 dex (90% of the galaxies lie within $\pm$0.12 dex). The velocity dispersion σ_c is measured in a fixed physical aperture defined by an angular aperture $3\rlap{.}''4$ in diameter at Coma (Jorgensen et al. 1995b), the intermediate axis effective radius is r_e, and the mean surface brightness ($\mu_e = m + 5\log r_e + 2.5\log 2\pi$) is corrected to zero redshift (Jorgensen & Franx 1994). When analyzing individual galaxies it is useful to view the FP as a means of predicting the surface brightness the galaxy will have at zero redshift. If we again hold the slopes fixed, we find that the FP relation for the zero-redshift surface brightness is

$$\left(\frac{\mu_{F606W}^{FP}(0)}{\text{mag/arcsec}^2}\right) = -3.76\log\left(\frac{\sigma_c}{\text{km s}^{-1}}\right) + 3.03\log\left(\frac{r_e}{h_{50}^{-1}\text{kpc}}\right) + 26.25 \tag{2}$$

with a scatter of 0.23 mag/arcsec^{-2} in the local JFK sample (90% of the galaxies lie within $\pm$0.37 mag/arcsec^{-2}). The covariances of $\log r_e$ and μ_e make the variable combination $\log r_e - 0.33\mu_e$ appearing in the expressions for the FP insensitive to measurement errors, with uncertainties 5–10 times smaller than those in either $\log r_e$ or μ_e alone (see Jorgensen, Franx & Kjaergaard 1993).

2.2. Using the FP to Measure Galaxy Evolution

We will use the FP to study the surface brightness evolution of early-type galaxies. We observe galaxies through a series of filters j from which we can compute the surface brightness $\mu_j(z)$. The surface brightness evolves as

$$\mu_j(z) = \mu_j(0) + 10\log(1+z) + e_j(z) + k_j(z), \tag{3}$$

where the first redshift term is the $(1 + z)^4$ cosmological dimming, the second is the evolution correction for filter j in the galaxy rest frame, and the third term is the K-correction from the rest frame to the observed frame. We estimate $\mu_j(0)$ using the FP (eqn. 2) and the angular diameter distance $D_A(z)$ to the galaxy. The difference between the observed surface brightness and the estimated zero-redshift surface brightness, $\mu_j^{FP}(0)$, is a direct measurement of the evolution and K-correction terms for band j,

$$e_j(z) + k_j(z) = \mu_j(z) - \left(\mu_j^{FP}(0) + 10\log(1 + z) \right). \tag{4}$$

We will not interpolate between filters to eliminate the K-correction (as is done for most of the cluster studies) because our filter coverage is incomplete. A spectrophotometric model is needed to interpret the results in either case, so the only advantage to measuring $e_j(z)$ or the mass-to-light ratio at a fixed rest wavelength is pedagogic. The values of e_j and k_j depend on the cosmological model only through the angular diameter distance used to estimate the physical effective radius (and the velocity dispersion for the gravitational lenses). We will not, at present, include a model for the modest changes in the slope of the FP with wavelength because there is still considerable uncertainty in its measurement (see Pahre, de Carvalho & Djorgovski 1998ab).

2.3. Lensed Image Separations and Stellar Velocity Dispersions

For almost all lenses we need to estimate the central velocity dispersion σ_c from the geometry of the lensed images rather than using direct measurements. The image separation $\Delta\theta$ accurately determines the mass of the lens on that scale, which we must convert into an estimate of σ_c.[3] The best explored model is the dark matter or singular isothermal sphere (SIS) mass model. In the SIS model the image separation, $\Delta\theta = 8\pi(\sigma_D/c)^2 D_{LS}/D_{OS}$ where D_{LS} and D_{OS} are the angular diameter distances from the lens to the source and from the observer to the source respectively, is set by the velocity dispersion of the dark matter σ_D rather than the central velocity dispersion of the stars σ_c. Dynamical models of nearby early-type galaxies in SIS halos by Kochanek (1994) demonstrated that the two have nearly identical values, with $\langle \sigma_c - \sigma_D \rangle = (8 \pm 26)$ km s^{-1}. Models for the observed distribution of image separations (Kochanek 1996, Falco et al. 1998) yield $\sigma_{c*} \simeq \sigma_{D*} \simeq (225 \pm 25)$ km s^{-1} for the velocity dispersion of an L_* galaxy. Thus, we estimate the stellar velocity dispersion by

$$\sigma_c = \frac{225}{f} \left(\frac{\Delta\theta}{2\rlap{.}''91} \frac{D_{OS}}{D_{LS}} \right)^{1/2} \text{ km s}^{-1}. \tag{5}$$

which is normalized for an L_* galaxy. We include a factor $f = \sigma_D/\sigma_c \simeq 1.0 \pm 0.1$ for the uncertainties in the dynamical normalization.[4] Measurement errors in $\Delta\theta$ are well under 5% even

---

[3] The image separation $\Delta\theta$ is defined to be twice the critical radius of the best fitting singular isothermal sphere (SIS) in an external tidal shear model for the image positions using a simple source plane χ^2. This definition is closely related to the mass enclosed by the images and roughly equal to the average distance of the lensed images from the lens galaxy. Using the maximum image separation leads to larger residuals in the FP.

[4] For the historically minded, the factor f is identical to the correction factor originally introduced by Turner, Ostriker & Gott (1984), who advocated a value of $f = (3/2)^{1/2} = 1.22$ based on simple models of luminous galaxies

in the worst cases, and can be ignored compared to the systematic errors in converting $\Delta\theta$ into a velocity dispersion. Note that a 14% change in f is needed before the shift in the FP matches its local thickness. It is important to remember that the dark matter model, despite its simplicity, is not used merely for analytic convenience. It is the mass model that is most consistent with the lensing data (e.g. Kochanek 1995), local stellar dynamics of ellipticals (e.g. Rix et al. 1997) and the X-ray halos of ellipticals (e.g. Fabbiano 1989).

We also experimented with constant M/L dynamical models even though they are less physically plausible. We assumed the mass and luminosity distribution could be approximated by a Hernquist (1990) model, and computed constant isotropy parameter β (Binney & Mamon (1982), $\beta = 0$ is isotropic, $\beta = 1$ is purely radial) stellar dynamical models normalized to have the observed mass inside the Einstein ring of the lens. For Hernquist radius a and total mass M_T, the central velocity dispersion averaged over aperture R_v can be written as $\sigma_c^2 = (GM_T/a)f_1(R_v/a)$ where $f_1(R_v/a)$ is a dimensionless function of the dynamical model. The lensing mass of $M_L = \pi\Delta\theta^2\Sigma_{crit}/4$ is independent of the dynamical model and the mass distribution and it is related to the total mass by $M_L = M_T f_0(\Delta\theta/2a)$ where $f_0(\Delta\theta/2a)$ is the fraction of the total mass inside projected radius $\Delta\theta/2$. Thus, the central velocity dispersion is determined by

$$\sigma_c^2 = 4\pi \left(\frac{c}{7200}\right)^2 \left(\frac{\Delta\theta}{1\rlap{.}''0}\right)^2 \left(\frac{1\rlap{.}''0}{a}\right) \frac{D_{OS}}{D_{LS}} \frac{f_1(R_v/a)}{f_0(\Delta\theta/2a)}. \tag{6}$$

The expression is independent of H_0 because the distance dependent terms appear only in ratios. We adopt the standard dynamical aperture of $2R_v = 3\rlap{.}''4$ at the Coma cluster from JFK. We set the Hernquist radius to $a = 0.551r_e$ (Hernquist 1990) and we will consider both isotropic ($\beta = 0$) and fairly radial ($\beta = 0.5$) dynamical models with solutions determined using the Jeans equations. The isotropy assumptions are restrictive, and more sophisticated models allow considerable freedom in the central velocity dispersion (see Romanowsky & Kochanek 1999).

2.4. HST Photometry of Lens Galaxies

We considered a sample of 30 lenses observed with either WFPC2 or NICMOS in the V=F555W, F606W, R=F675W, F702W, F791W, I=F814W, J=F110W, H=F160W and K=F205W filters. A summary of the observations is presented in Table 1. Of these 30 systems, 10 are missing spectroscopic lens redshifts and 6 are missing spectroscopic source redshifts. We regard the V, I and H filters as our standards and we will frequently use spectrophotometric models to convert measurements in the other filters to the standard filters. We assumed Vega-normalized zero-points (1 count/s in an infinite aperture) of 21.88, 21.80 and 22.47 mag for the F205W, F160W, and F110W NIC2 filters, 21.51 for the F160W NIC1 filter (see Lehár et al. 2000), and 21.69, 21.57, 22.47, 22.08, 22.93 and 22.57 mag for the F814W, F791W, F702W, F675W, F606W and F555W filters for a gain of 7 (Holtzman et al. 1995, corrected to infinite aperture). Our full data reduction and analysis procedures are detailed in Lehár et al. (2000). For each lens galaxy

---

in dark matter halos. A normalization this high is inconsistent with both the dynamics of nearby galaxies and the observed distribution of image separations.

we determined the intermediate axis effective radius on the image having the best signal-to-noise for the galaxy. With the scale and shape of the lens galaxy fixed, we determined the surface brightnesses for the remaining filters. The uncertainties were estimated as the quadrature sum of a statistical term from separate fits to the individual subexposures, a PSF uncertainty term from fits with multiple PSFs, and a modeling uncertainty term from the difference between two independent modeling codes. The uncertainties were separately recorded for colors, magnitudes, and the variable combination appearing in the FP. In many cases, however, the magnitude and surface brightness uncertainties are dominated by zero-point uncertainties of 0.03–0.05 mag. Table 3 presents the photometric data for the sample we consider. We include the uncertainties in the strongly correlated quantities $(\mu_e - 3.03 \log \theta_e)$ appearing in the FP equations. In our analysis we correct the photometric data for Galactic extinction using the extinction estimates of Schlegel, Finkbeiner & Davis (1998) and an $R_V = 3.1$ extinction curve.

Of the 41 lenses for which we have photometry, we excluded 11 from the present survey. B 0218+357, RXJ 0921+4528, B 1600+434 and PKS 1830–211 have late-type lens galaxies.[5] Where the bulge of a late-type galaxy dominates the lensing, as in Q2237+0305, the bulge should lie on the fundamental plane and there is no reason for excluding the system. The lens galaxy remains undetected in Q 1208+1011 (Lehár et al. 2000), and the high contrast between the quasar images and the lens galaxy leads to poor lens galaxy photometry in QJ 0158–4325 (CTQ414), SBS 0909+532, H 1413+117 and FBQ 1633+3134. In MG 0751+2716 and B 1933+507 we are unable to reliably decompose the image into source and lens contributions. B 2114+022 (Jackson et al. 1998a) has two possible primary lens galaxies and the astrometric alignment of the lensed radio sources with the galaxies is still uncertain. We expect 10-20% of lenses to be late-type galaxies in the absence of any population evolution (e.g. Fukugita & Turner 1991, Maoz & Rix 1993, Kochanek 1993, 1996). Hence, the number of lenses we have dropped from the analysis is consistent with no number evolution in the early-type population to $z = 1$.

2.5. Spectrophotometric Modeling

We use the GISSEL96 version of the Bruzual & Charlot (1993) spectral evolution models to interpret the results. The models were computed for $H_0 = 65$ km s^{-1} Mpc^{-1} and three cosmological models (a flat cosmology with $\Omega_0 = 1$, a flat cosmology with $\Omega_0 = 0.3$ and $\lambda_0 = 0.7$, and an open cosmology with $\Omega_0 = 0.3$). We initially considered three star formation histories: an instantaneous burst in which all stars form at redshift z_f, an extended burst in which star formation starts at z_f and continues at a constant rate for 1 Gyr, and an exponentially decaying star formation starting at redshift z_f with a 1 Gyr e-folding time. However, we found that the interpretation was largely independent of the details of the star formation history and we restricted our presentation to the instantaneous burst model because it makes the interpretation of z_f straightforward. The results for the extended or exponential burst models will match the instantaneous burst models if the end of the star formation epoch (roughly z_f plus 1 Gyr) is

---

[5] We also know that B 0218+357, B 1600+434 and PKS 1830–211 are dusty (see Falco et al. 1999), and that B 0218+357 and PKS 1830–211 contain dense molecular gas (see Menten, Carilli & Reid 1999 and references therein).

matched to the instantaneous burst redshift. In most cases we used a solar metallicity model ($Z_\odot = 0.02$), although for redshift estimation (§5) we used a range of models from $Z_\odot/4$ to $4Z_\odot$ to provide a range of galaxy colors at fixed age.

2.6. Direct Comparison to Cluster Galaxies at Similar Redshifts

The comparison to the spectrophotometric models is subject to systematic problems in both the models and the data analysis. By directly comparing the field, lens population to the rich cluster population we can avoid these systematic problems. We obtained the archival WFPC2 images of the rich clusters studied by van Dokkum & Franx (1996), Kelson et al. (1997), van Dokkum et al. (1998a) and Pahre, Djorgovski & de Carvalho (1999ab). We extracted the early-type galaxies for which velocity dispersions were measured and redetermined their photometric properties using our standard methods (Lehár et al. 2000) to obtain a comparison sample of 50 early-type galaxies in very dense environments (see Tables 2 and 4). Since the photometric reductions and zero-points are identical for the lens and cluster samples, any differences between the samples must be caused either by differences in their star formation histories or by the methods for estimating the central velocity dispersions of the lens galaxies (see §6). Table 4 presents the data for the cluster galaxies. For Cl1358+62 (Kelson et al. 1997), MS2053–04 (Kelson et al. 1997) and MS1054–03 (van Dokkum et al. 1998a), where we are fitting the same data, we agree with the published effective radius estimates to accuracies of (mean±dispersion) 0.06 ± 0.14 dex, -0.02 ± 0.10, and -0.05 ± 0.06 dex respectively despite the different procedures used to determine the effective radius in each analysis. Kelson et al. (2000) refit the Cl1358+62 galaxies, with a change in the effective radius of -0.04 ± 0.07 relative to their previous results, and in closer agreement with our results (0.02 ± 0.09). The importance of these differences is further reduced by the insensitivity of the quantities appearing in the FP to errors in r_e.

3. The Colors of Lens Galaxies

Keeton et al. (1998) made the first systematic survey of the colors of lens galaxies, finding that most were consistent with the predictions for passively evolving early-type galaxies – blue or star-forming lenses are rare. With the CASTLES photometry we can now examine both the optical and infrared colors of the galaxies, although the incomplete and inhomogeneous WFPC2 observations mean we must still use the spectrophotometric models to transform the data for display. Figure 1 illustrates the I–H and V–I colors of the individual lens and cluster galaxies as compared to the instantaneous burst models.

At low redshift, both the lens and the cluster galaxies have colors consistent with either the low ($z_f = 1$) or the high ($z_f = 3$) formation epochs, particularly if there is freedom to adjust the metallicity. Above $z = 0.5$ the models begin to diverge, and it becomes trivial to distinguish between the two formation epochs by $z = 1.0$. We will adopt the solar metallicity, $z_f = 3$, instantaneous burst as our standard star formation history. The models are a good global match to the colors of both the lens and cluster galaxies. If we estimate the difference between the
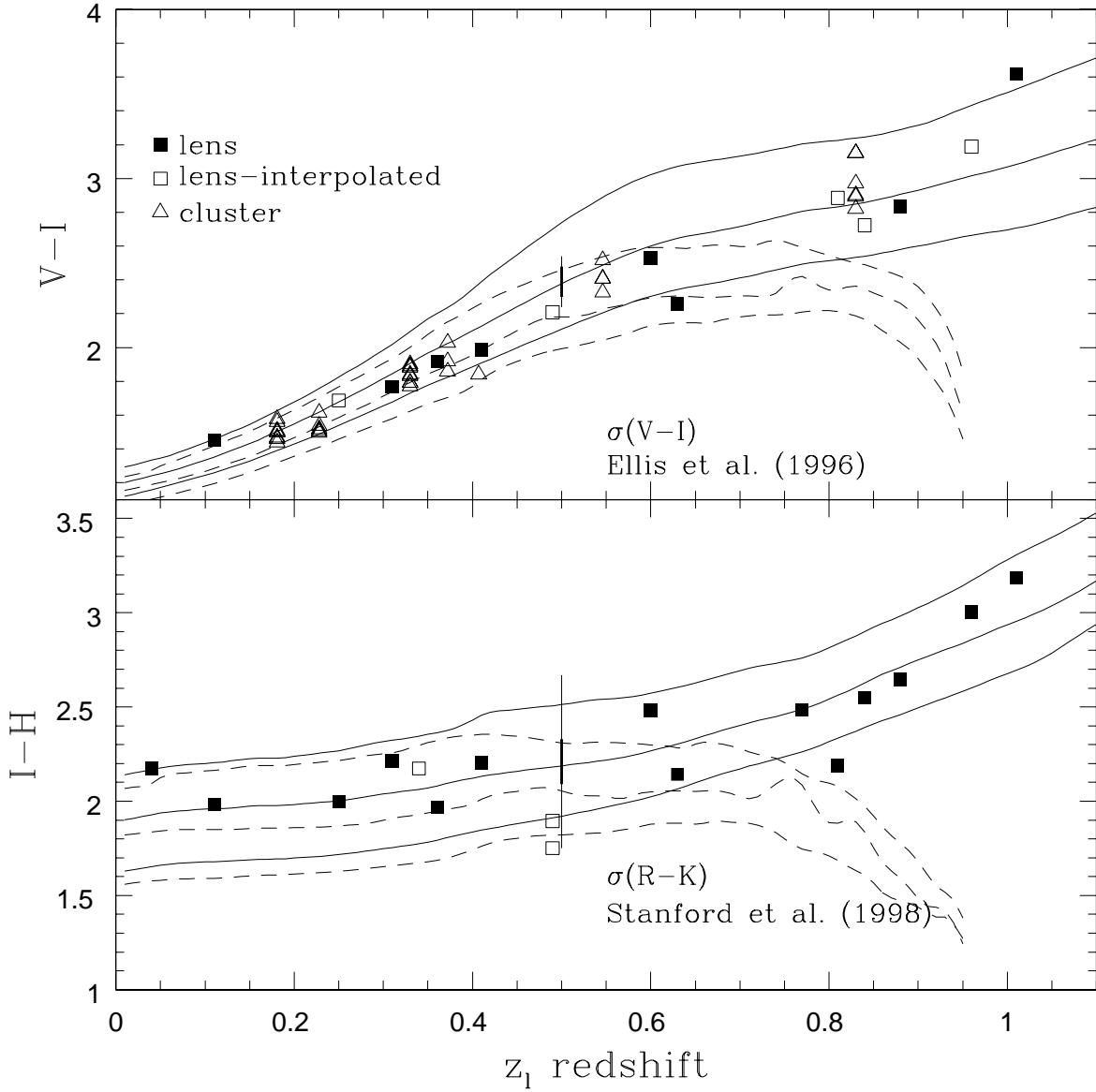
Fig. 1.— V–I (top) and I–H (bottom) colors as a function of redshift for the lens and cluster galaxies. Only the lenses with spectroscopic redshifts are included. The heterogeneous optical filters for the lens data are interpolated to V=F555W or I=F814W as needed using the solar metallicity, $z_f = 3$ instantaneous burst model. The solid (dashed) lines show the predicted V–I and I–H colors for the $z_f = 3$ ($z_f = 1$) instantaneous burst spectrophotometric models with metallicities of $Z = 0.4Z_{\odot}$ (bottom), $Z_{\odot}$ (middle) and $2.5Z_{\odot}$ (top). The error bars at $z = 0.5$ show the scatter in the V–I and R–K colors observed for rich clusters at $z \simeq 0.5$ by Ellis et al. (1997) and Stanford et al. (1998). The heavy error bars are the scatter at fixed luminosity, and the light error bars are the additional scatter due to the correlations between luminosity and color in a sample averaged over a wide range of luminosities. Only lenses with known lens redshifts are included.

observed optical colors and the model colors for the same redshift, the mean color difference and its dispersion relative to the models is -0.03 ± 0.11 mag for the V–I color of the cluster galaxies and -0.05 ± 0.22 mag for the V–I and R–I color differences of the lens galaxies. The color dispersion includes that from the measurement errors, which are generally larger for the lenses. For comparison, the color dispersion for the large samples of rich cluster galaxies at $z \simeq 0.5$ studied by Ellis et al. (1997) and Stanford et al. (1998) is 0.13 mag in V–I. We do not have infrared magnitudes for the cluster galaxies, but the optical (V, R or I) to infrared (H) color difference and its dispersion is -0.02 ± 0.25 mag, compared to a dispersion of 0.29 mag in the R–K color for the large cluster samples (Stanford et al. 1998).

4. The Fundamental Plane of Lens Galaxies

We can show that the lens galaxies lie on a coherent fundamental plane by evolving their properties forward in time and placing them on the present day FP. The photometric transformations depend on both the star formation epoch (z_f) and the cosmological model (Ω_0 and λ_0), as illustrated in Figure 2 for the lens galaxies and in Figure 3 for the cluster galaxies. Where we possess data in multiple filters, we have used the error-weighted average of the estimates, and for the lens galaxies lacking spectroscopic redshifts we have estimated the redshifts using the methods in §5.

It is clear from Figure 2 that the lens galaxies will lie on the local FP if enough time has passed since the star formation epoch. This implies a star formation redshift $z_f \gtrsim 2$ and a low matter density cosmology. As van Dokkum & Franx (1996) noted for the cluster early-type galaxies, it is difficult to reconcile an $\Omega_0 = 1$ cosmology with a reasonable star formation epoch ($z_f \lesssim 5$) unless significant changes are made in the initial mass function (IMF) of the stars. More remarkably, we see by comparing Figures 2 and 3 that the FP of the lens galaxies is nearly identical to that of the cluster galaxies. The cluster galaxies show smaller discrepancies for a low star formation redshift, but this is due to the lower mean redshift of the cluster sample.

We can quantify the differences using the mean offset of samples from the local FP, $\Delta = \langle \log(r_e/r_e^{FP}) \rangle$, and the dispersion of the sample around the mean offset, σ_Δ. For a population of galaxies of the same age, we would find $\Delta = 0$ and a minimum in σ_Δ when the model age matched the true age. For a distribution of galaxy ages we would find $\Delta = 0$ and a minimum in σ_Δ near the average age, but the width of the distribution would be wider than that of the local FP. In fact, the minimum dispersions of the two samples are identical, $\sigma_\Delta = 0.11$, and larger than that of the local JFK sample where $\sigma_\Delta = 0.07$. They are larger than the estimated uncertainties in the inputs to the calculation ($\log r_e - 0.33\mu_e$ and $\Delta\theta$ or σ_c), which can be caused either by physics (the galaxy age distribution) or systematic errors (zero-points, averaging over heterogeneous filters, or the weak wavelength dependence of the FP). A physical explanation requires only a modest admixture of younger galaxies to a largely old population. For example, if fraction ξ of the galaxy population formed at $z_f = 1$ and fraction $1 - \xi$ formed at $z_f = 3$, we could explain the measured offsets and dispersions by an FP whose intrinsic width matches the local FP but has a $\xi = 13\%$ ($\xi = 35\%$) young galaxy fraction for the lens (cluster) sample in the $\Omega_0 = 0.3$ flat cosmology. The lower mean galaxy redshift in the cluster sample allows a larger young galaxy fraction.
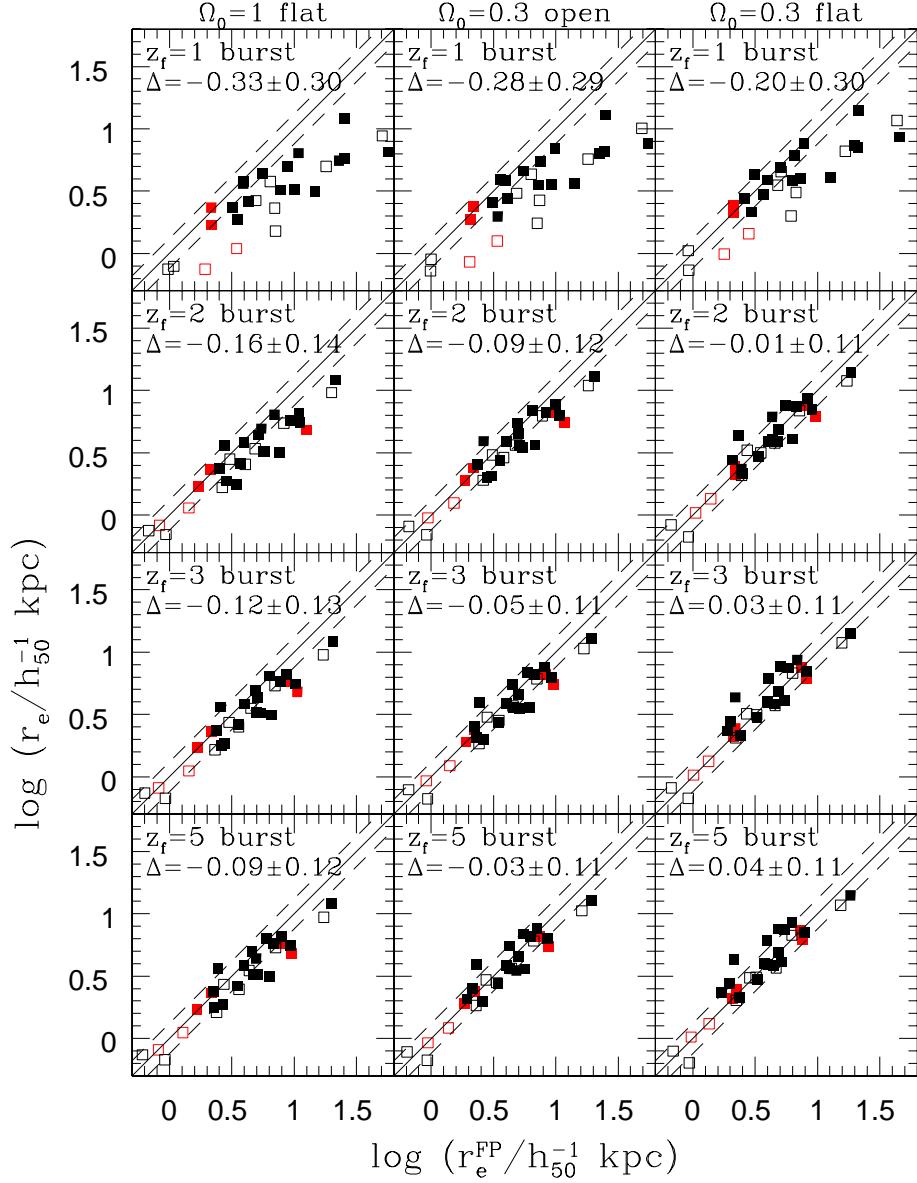
Fig. 2.— The FP of lens galaxies transformed to zero redshift. The cosmologies (from left to right) are the $\Omega_0 = 1.0$ flat, $\Omega_0 = 0.3$ open and $\Omega_0 = 0.3$ flat models. The solar metallicity instantaneous burst star formation history is used with star formation redshifts (from top to bottom) of $z_f = 1$, 2, 3 and 5. The filled squares are for the lenses with known redshifts and for the open squares we have used the color and the FP to estimate the lens redshifts (see §5). The solid line marks the FP of the local comparison sample; 90% of the galaxies in the local JFK sample lie between the dashed lines. The mean residual ($\Delta = \langle \log(r_e/r_e^{FP}) \rangle$)) and its dispersion are shown in the upper left corner of each panel. These are calculated using only the systems with known lens redshifts. Lenses without spectroscopic redshifts are included using the methods of §5 to estimate the lens redshift *assuming the cosmological model and spectrophotometric model of that panel.*
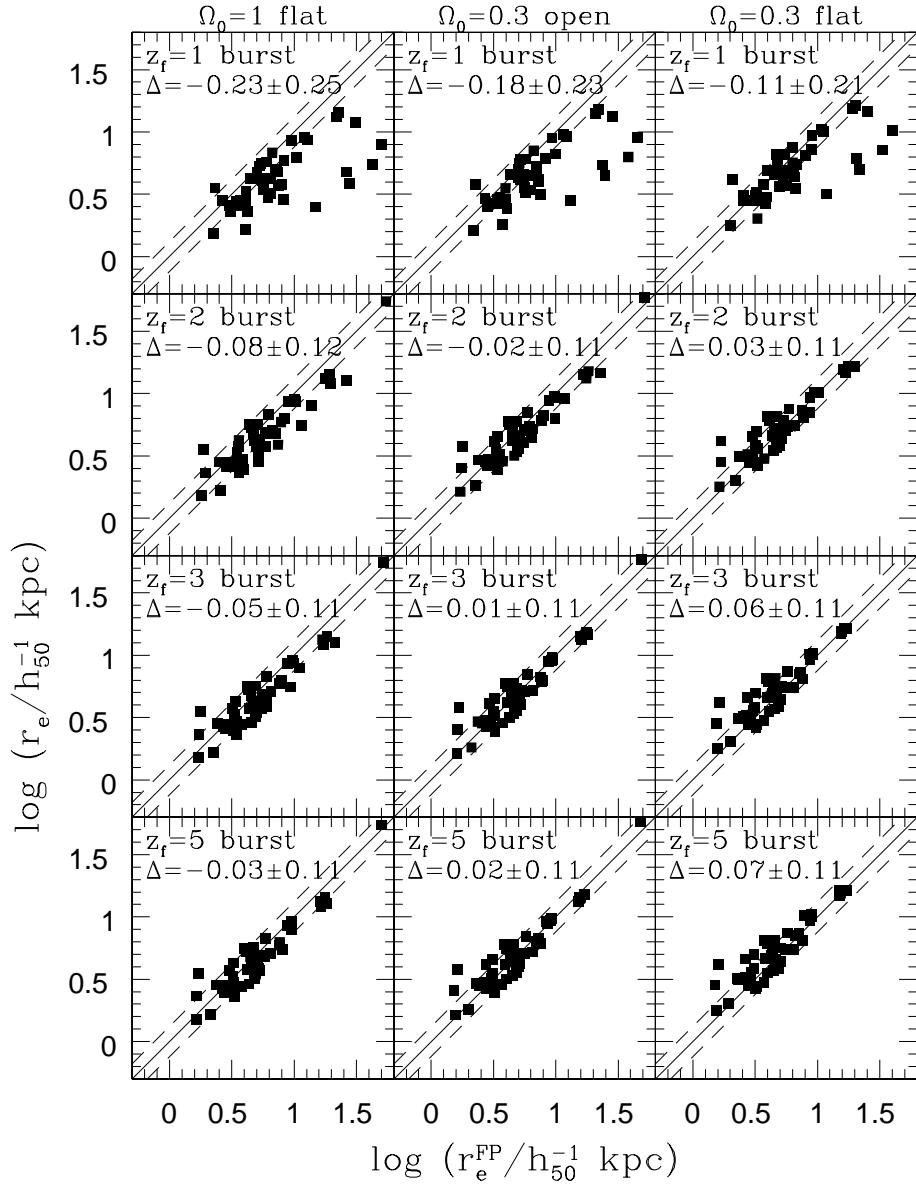
Fig. 3.— The FP of cluster galaxies transformed to zero redshift. Same cases as in Figure 2.

The similar evolution of the cluster and lens galaxies is more reliably demonstrated by the equivalence of the dispersions than by that of the offsets for the same assumed formation epoch because the offset Δ is affected directly by systematic errors in estimating the stellar velocity dispersion from the image separations using eqns. (5) or (6). In particular, we parameterized the uncertainty for the SIS model by the ratio $f = \sigma_D/\sigma_c$. Changing the value of this factor changes the offset Δ by $1.24 \log f = \pm 0.12$ given the uncertainties estimated from stellar dynamics and the distribution of lens separations ($f = 1.0 \pm 0.1$). Such freedom is sufficient to significantly alter the formation redshift implied by the value of Δ up to a limit such that $z_f \gtrsim 1.5$, but changing it has no effect on the dispersion σ_Δ or the estimate of a possible young galaxy fraction ξ. We discuss the dynamical normalization of the lenses further in §6, and we measure the rate of galaxy evolution independent of the dynamical normalization in §7.

5. Redshift Estimation

Unmeasured lens redshifts are a major limitation on the use of gravitational lenses to study cosmology (see Kochanek 1992, Helbig & Kayser 1996, Kochanek 1996), so it is important to develop a reliable, accurate method for estimating lens galaxy redshifts. The redshift uncertainties from estimates based on the Faber-Jackson (1976) relation or gravitational lens statistics are too broad (see Kochanek 1992), even though Keeton et al. (1998) found that lens galaxy luminosities follow the expected correlations. The reduced scatter in the FP compared to the Faber-Jackson relationship should make it a better means of estimating lens redshifts. Moreover, we now have accurate colors for many of the lens galaxies, and photometric redshifts should work very well because most lens galaxies are intrinsically red, early-type galaxies.

We estimate the redshifts using the formalism of the fundamental plane because it leads to a method that works in the absence of any color information. For each filter j we use a spectrophotometric model and the FP relations (eqn. 1) to estimate the physical effective radius, $r_e^{(j)}(z_l, z_s)$, and then compare it to the observed physical effective radius, r_e. The estimates of the effective radius derived from the FP ($r_e^{(j)}$) depend on the lens redshift, the source redshift and the spectrophotometric model, while the estimate of the physical effective radius (r_e) depends only on the lens redshift through the angular diameter distance. When we match all the estimates $r_e^{(j)}$ we are obtaining a color redshift, and when we match $r_e^{(j)}$ with r_e we are obtaining a fundamental plane redshift. A χ^2 statistic measures the goodness of fit given the magnitude uncertainties and the thickness of the fundamental plane.

Figure 4 illustrates the method for two systems and a particular model (a $z_f = 3.0$ solar metallicity instantaneous burst). A perfect example of the method is PG 1115+080, where the galaxy lies precisely on the FP with colors matching the spectrophotometric model at the true lens redshift. An example of a self-consistent, but incorrect, redshift determination is shown by B 1608+656. As in PG 1115+080, there is a redshift where the galaxy lies precisely on the FP with colors matching the model, but it is significantly offset from the true lens redshift and the estimated uncertainty is far less than the actual error. The B 1608+656 lens galaxy has both [O II] emission and a weak $4000\mathring{A}$ break (Myers et al. 1995), indicating some ongoing star formation. If we use a $z_f = 1$ spectrophotometric model instead of a $z_f = 3$ model, then the lens
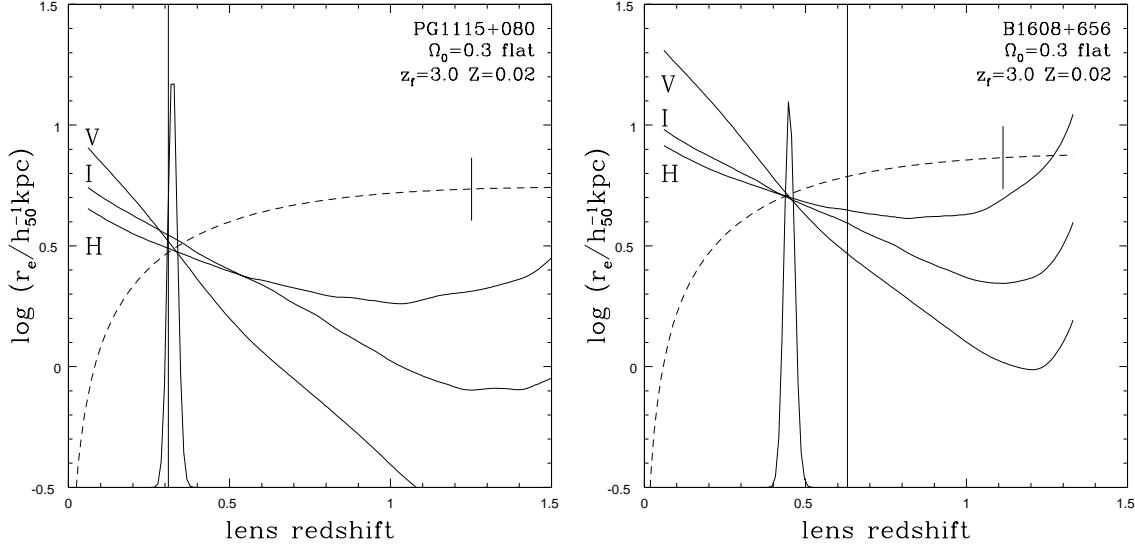
Fig. 4.— Examples of redshift estimation for the $z_l = 0.31$ lens PG 1115+080 (left) and the $z_l = 0.63$ lens B 1608+656 (right). The dashed curve is the physical effective radius r_e as a function of redshift. The errorbar on the dashed curve would encompass 90% of the galaxies on the local FP. The solid curves are the effective radii estimated using the FP $(r_e^{(j)})$ using the V, I and H surface photometry of the lens galaxy and assuming a solar metallicity, a $z_f = 3$ instantaneous burst model and an $\Omega_0 = 0.3$ flat cosmological model. A vertical line marks the spectroscopic lens redshift, and the "Gaussian" distribution shows the likelihood of fitting the data $(\propto \exp(-\chi^2/2))$. A galaxy lies on the FP when a solid curve crosses the dashed curve, and the galaxy colors match the spectrophotometric model when all the solid curves intersect.
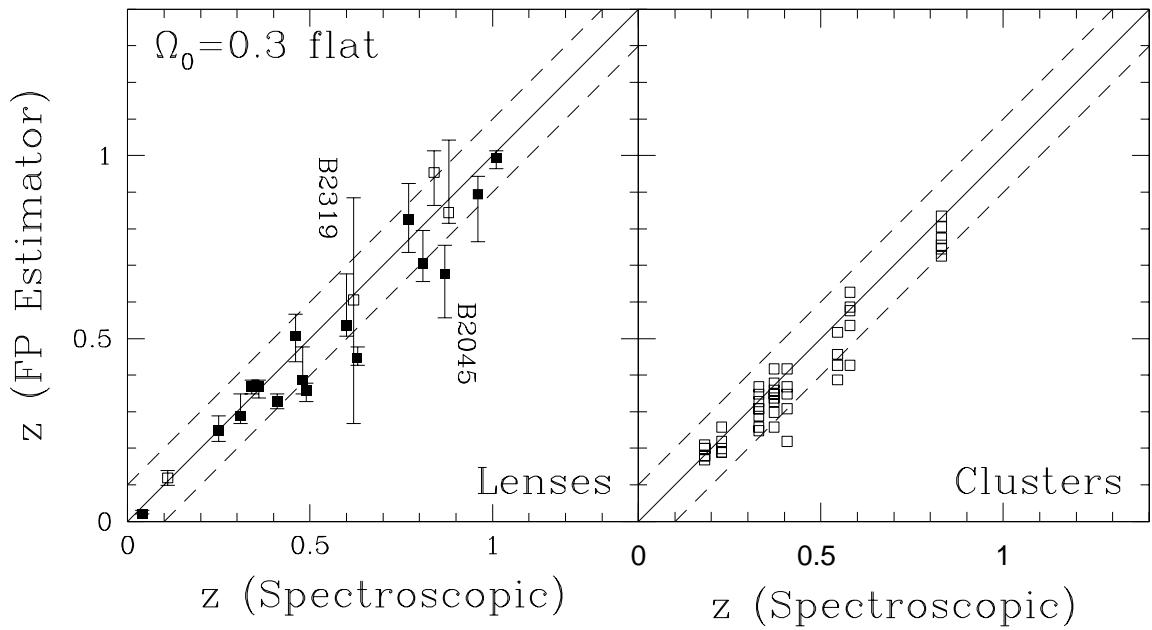
Fig. 5.— The FP redshift estimates compared to the spectroscopic redshifts. The left (right) panel shows the results for the lens (cluster) galaxies. For the lens galaxies, solid (open) points are used for lenses where the source redshift is known (unknown). The dashed lines are offset by $|\Delta z| = 0.1$ to illustrate the desired accuracy. We have only H-band data for the labeled lenses with large redshift uncertainties (B 2045+265 and B 2319+052).

both lies on the FP and matches the model colors at its true redshift. There are few such lens galaxies, consistent with the low young galaxy fraction we estimated in the previous section. For both of these systems we would have obtained the same redshift estimate from any single filter (no color information) just from the requirement that the galaxy lie on the FP. Such single filter redshift estimates work best at low redshift, where the angular diameter distance changes rapidly, or with optical filters, where the K-correction changes rapidly. The accuracy will be poor given only an infrared observation of a lens galaxy at $z_l \gtrsim 0.5$ where both the distance and the surface brightness vary slowly with redshift.

We determined the final redshift estimates by fitting each lens using $z_f = 3$ instantaneous burst models with a range of metallicities ($0.4Z_\odot$ to $2.5Z_\odot$) in an $\Omega_0 = 0.3$ flat cosmological model. The results are insensitive to the cosmological model, using a range of metallicities (a range of colors at fixed age) significantly improved the accuracy, and using a range of star formation epochs ($z_f = 1$ to $z_f = 3$) decreased the accuracy. For each lens we found the model and lens redshift which best fit the data and then estimated the uncertainties by the redshift range such that the change in the χ^2 statistic satisfied $\Delta\chi^2 < 4$ including variations in the metallicity. The results are illustrated in Figure 5. Formally, the uncertainty estimates are 2σ limits, but many of the errors are systematic rather than statistical and the $\Delta\chi^2 < 4$ error estimate seems to match the actual scatter seen in Figure 5. The mean and dispersion of the redshift differences are $\langle z_{FP} - z_l \rangle = -0.04 \pm 0.09$ for the lenses and $\langle z_{FP} - z_c \rangle = -0.03 \pm 0.06$ for the clusters. The redshift estimates are presented in Table 5. Note that the redshifts derived in Figure 4 using a particular spectrophotometric model will differ from the final estimates in Figure 5 and Table 5 which statistically average over a range of models.

6. Dynamical Normalization

We next consider the dynamical normalization of the lens models using the FP as a tool to probe the relationship between σ_* and $\Delta\theta$. This is a substantial digression from the question of galaxy evolution, and in §7 we will rederive the evolution of the galaxies in a way which is clearly independent of uncertainties in the normalization. Nonetheless, consideration of gravitational lenses and the FP would be incomplete without further discussion of normalization. Ideally we would like to have a large sample of gravitational lenses with direct velocity dispersion measurements. In fact, velocity dispersions have been measured for four gravitational lenses Q0957+561 (Tonry & Franx 1999, Falco et al. 1997, Rhee 1991), PG1115+0808 (Tonry 1998), MG1549+3047 (Lehár et al. 1996) and the bulge of Q2237+0305 (Foltz et al. 1992). Using the aperture correction model of Jorgensen et al. (1995) we estimated that the velocity dispersions of the four lens systems in the standard $3''.4$ aperture at Coma are $\log(\sigma_c/ \text{ km s}^{-1}) = 2.484 \pm 0.015$, 2.460 ± 0.040, 2.384 ± 0.035, and 2.343 ± 0.061 respectively. The errors include the formal measurement error combined in quadrature with a generous uncertainty in the aperture definition. Unfortunately, two of these four systems are peculiar: Q0957+561 is the lens whose properties are most contaminated by the mass distribution of the cluster to which the lens galaxy belongs, and Q2237+0305 is a bright nearby spiral galaxy rather than a massive early-type galaxy. Nonetheless, we have three estimates of the velocity dispersion to compare: the directly measured stellar dispersions, σ_*; the estimates of the stellar dispersion from the image separation, $\sigma_{\Delta\theta}$, which will
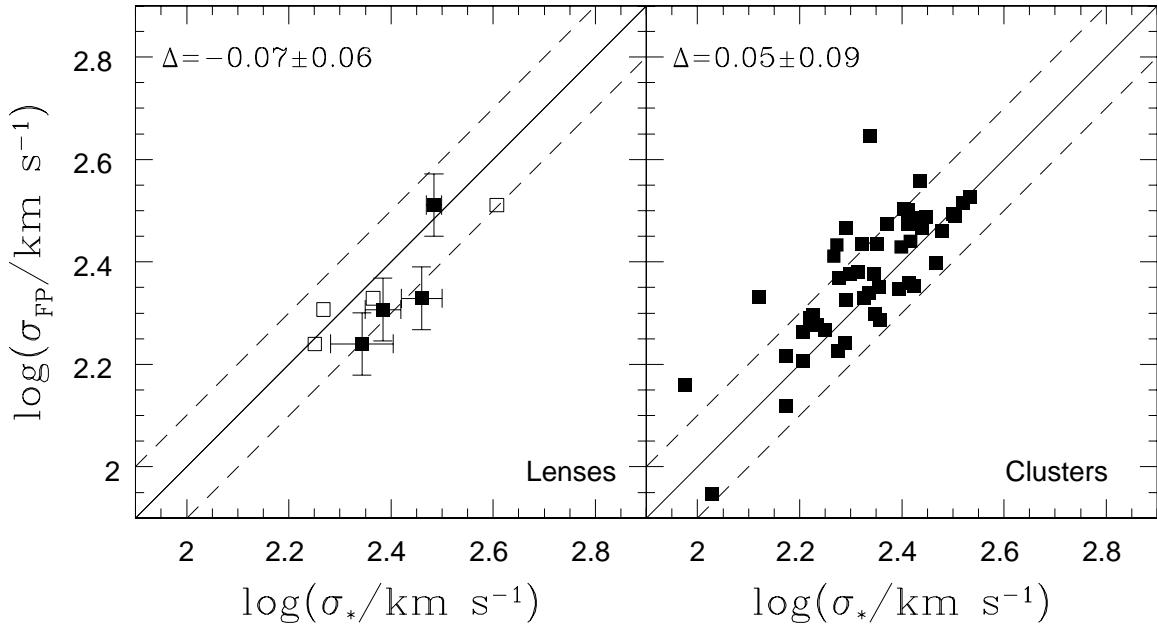
Fig. 6.— A comparison of central velocity dispersions, σ_*, and velocity dispersion predictions from the FP, σ_{FP}, for the lens galaxies (left) and the cluster galaxies (right). The lens galaxies are Q2237+0305, MG1549+3047, PG1115+080 and Q0957+561 (in order of increasing σ_*). For the lenses, the velocity dispersions estimated from the image separations, $\sigma_{\Delta\theta}$, are shown as open points. The dashed lines would encompass 90% of the galaxies in the local JFK sample. The mean offset $\Delta = \langle \log \sigma_{FP} - \log \sigma_* \rangle$ and its dispersion are shown in the upper left corner. The value of σ_{FP} was computed for the solar metallicity, $z_f = 3$ instantaneous burst model and an $\Omega_0 = 0.3$ flat cosmological model. Note that the right panel is the same as the equivalent model in Figure 3.
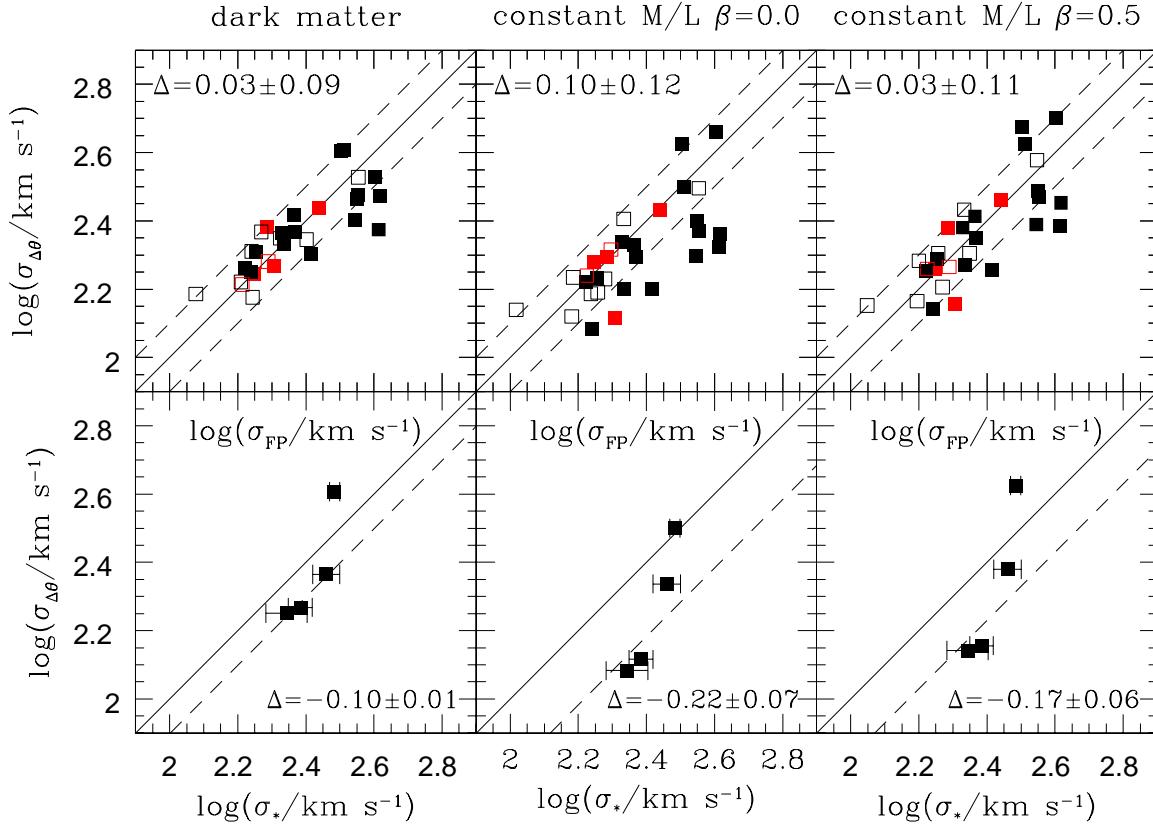
Fig. 7.— A comparison of the velocity dispersions estimated from the lens model, $\sigma_{\Delta\theta}$, to the measured stellar dispersion, σ_* (bottom), and to the dispersion estimated from the FP, σ_{FP} (top). The value of $\sigma_{\Delta\theta}$ is estimated from the lens geometry using the dark matter (left), isotropic constant M/L (middle), and radially anisotropic constant M/L (right) dynamical models. In the top panels, $\Delta = \langle \sigma_{FP} - \sigma_{\Delta\theta} \rangle$ to match the form used in Figures 2 and 3. In the bottom panels, $\Delta = \langle \sigma_{\Delta\theta} - \sigma_* \rangle$, but we exclude Q 0957+561 because of the effects of the cluster on $\sigma_{\Delta\theta}$. The values are the mean and the dispersion about the mean. The cosmological and spectrophotometric models are the same as in Figure 6. In the upper panel the dashed curves would encompass 90% of the galaxies in the local JFK sample, and in the lower panel the dashed curve is the mean offset excluding Q 0957+561.

depend on the dynamical model and (weakly) on the cosmological model; and the FP estimate of the velocity dispersion, σ_{FP}, which depends on the cosmology and the spectrophotometric model.

We first compare the measured stellar dispersions to the FP predictions (σ_* and σ_{FP}) because this comparison is independent of the dynamical model used for the lenses. Figure 6 shows the comparison for both the lens and cluster galaxies assuming the solar metallicity, $z_f = 3$ instantaneous burst model. In the local JFK sample the dispersion of the FP measured in terms of velocity dispersions is 0.06 dex with 90% of the galaxies lying within 0.1 dex. For the clusters, Figure 6 is simply the comparison made in Figure 3 plotted in terms of velocity dispersion rather than effective radius. For the lenses this comparison is fundamentally different from that in §3 and Figure 2 because we are not using the lens geometry to estimate the velocity dispersion. If we estimate the offset by $\Delta = \langle \sigma_{FP} - \sigma_* \rangle$, then the velocity offset should be 0.8 of the effective radius offset measured in §3 because it is just a rearrangement of the terms in the FP defined by eqn. (1). To the extent that four points suffice to define the FP, we see that the lenses will also lie on the FP if we use the directly measured velocity dispersions, but that it is offset slightly from the estimate using $\sigma_{\Delta\theta}$ in §3.

For the lenses we can also compare the velocity dispersion estimated from the image separation, $\sigma_{\Delta\theta}$, to the observed stellar dispersions, σ_*, and the FP estimates, σ_{FP}, as shown in Figure 7. Here the results depend on the dynamical model, and we show the comparison for our standard dark matter model and the two constant M/L models (isotropic $\beta = 0$ and radially anisotropic $\beta = 0.5$). The dispersion in the FP (Figure 7, top) is roughly independent of the dynamical model, although the isotropic constant M/L model has a significant offset from the FP found using either the dark matter or radially anisotropic constant M/L model. The sense of the offset is that the isotropic model would require an older stellar population to match the local FP. The agreement between $\sigma_{\Delta\theta}$ and the measured stellar dispersions σ_* is significantly worse in the constant M/L models than in the dark matter model. In this comparison we must ignore Q 0957+561 where we know that the value of $\sigma_{\Delta\theta}$ is increased by the effects of the cluster containing the lens galaxy.

Although the offsets are smallest for the dark matter model, they still imply a marginally significant normalization change to $f \simeq 0.80 \pm 0.05$ rather than $f = 1.0 \pm 0.1$ (see §2.3). Such a change in the normalization requires either making the lens galaxies older or giving them more dark matter on the scale of the image separations than for the galaxies in rich clusters. It is, however, a sample of only 3 objects, one of which is the bulge of a nearby spiral rather than a massive early type galaxy. The low value of f also implies a separation distribution for the lenses which would be grossly inconsistent with the data.[6] Three of the four systems (Q 0957+561, PG 1115+080 and Q 2237+0305) have bright quasar images in the core of the galaxy whose emission complicates velocity dispersion measurements, and it is possible that the significance of the offset is exaggerated by underestimation of the uncertainties in the dynamical measurements. In §8 we provide a list of lenses with relatively high central surface brightnesses and minimal source contamination which could be used to improve the dynamical comparison. It would be

---

[6]The average image separation scales as $\langle \Delta\theta \rangle \propto f^2$, so a change from $f = 1$ to $f = 0.8$ reduces the mean image separation to 64% of its standard value.

best, however, to eliminate completely the effects of the normalization from the measurement of the evolution.

7. Galaxy Evolution

We can eliminate the apparent dependence of the evolutionary estimates on the dynamical normalization by abandoning the construction of the FP (as in §4) and instead calculate directly the E+K corrections as a function of lens redshift using eqn. (4). The information on galaxy evolution is contained in the changes in the corrections with redshift, and is independent of errors in the dynamical normalization. In doing so we only assume that the galaxies will evolve to lie on the local FP at $z = 0$. The resulting values for the E+K corrections are independent of the spectrophotometric model but depend on cosmology through the variations in cosmological distances. Note that the calculation of the evolutionary corrections only requires the existence of a coherent, thin FP for the local reference population. To condense the results we transformed the non-standard filters into the standard filters using the best fit spectrophotometric model.[7] Where the filter transformations lead to multiple estimates for a single lens, we decided to regard it as an additional means of estimating uncertainties. The surface brightness scatter of the FP is still significant (in the local JFK sample it is 0.23 mag), so we averaged the estimates from the individual galaxies in four redshift bins with edges at $z = 0.25$, 0.50 and 0.75 to produce the final numerical estimates presented in Table 6. The estimates of the E+K corrections depend on the spectrophotometric models only through the filter transformations and lens redshift estimates.

The evolution with redshift is shown in Figures 8 and 9, from which we can immediately draw five qualitative conclusions. First, the FP makes the evolution of the galaxies obvious. With the $(1 + z)^4$ cosmological dimming removed, the galaxies become rapidly fainter in the V band, have almost constant surface brightness in the I band, and become steadily brighter in the H band as the dominant term switches from the strong K-corrections at V band to the evolution corrections at H band. Second, the evolution is positive in all three bands, with the surface brightnesses steadily rising above the predictions for a non-evolving population. Third, as van Dokkum & Franx (1996) originally noted for the cluster galaxies, it is difficult to reconcile the measurements with the high $\Omega_0 = 1$ model because they require unphysically high star formation redshifts, $z_f > 10$. Fourth, neither sample is easily reconciled with low star formation redshifts ($z_f \lesssim 2$). Fifth, there are no obvious differences in the evolutionary histories of the early-type galaxies in low and high density environments.

Dynamical normalization errors have no effect on these evolution estimates, because they depend only on the changes in the E+K corrections with redshift. A change in the normalization factor f for the lenses shifts the estimates by $\Delta(e + k) = -3.76\Delta \log f$ for all filters and at all redshifts – changing f changes the zero-redshift mass-to-light ratio of the galaxies but not its evolution. If we fit the E+K corrections with a linear function of redshift, extrapolate to zero-redshift and estimate the difference between the estimates for the lens and cluster galaxies,

---

[7]We transformed J=F110W and K=F205W to H=F160W, F702W and F791W to I=F814W, and R=F675W and F606W to V=F555W.

we find $\Delta(e + k) = 0.05 \pm 0.25$ and -0.14 ± 0.24 for the V and I-bands respectively. The individual estimates of the $E + K$ corrections are all statistically consistent with zero at redshift zero. We know from the redshift evolution that the two populations have similar star formation histories, so the zero-redshift difference in the E+K corrections should provide an accurate means of estimating the normalization factor. Averaging the V and I-bands we obtain a final estimate of $f = 1.06 \pm 0.07$, which is consistent with our original estimates in §2 from either stellar dynamics or the average image separations of the lenses.

8. Conclusions

Most gravitational lens galaxies are early-type galaxies lying on the passively evolving fundamental plane, allowing us to measure the evolution rate of early-type galaxies in low density environments. We find that the stars constituting the lens galaxies must have formed at $z_f \gtrsim 2$ for an $\Omega_0 = 0.3$ flat cosmology. The required formation epoch increases for an open or higher matter density cosmology. Star formation histories with an extended burst or an exponentially decaying burst must form most of their stars before this redshift limit. More generally, we have directly measured the E+K corrections for "field" early-type galaxies in the V, I and H bands over the range $0 < z < 1$.

When we compare the lens galaxies to those in FP studies of rich clusters (van Dokkum & Franx 1996, Kelson et al. 1997, van Dokkum et al. 1998a, Pahre, Djorgovski & de Carvalho 1999ab, Jorgensen et al. 1999), we find no significant differences between the galaxies in the two environments. The high redshift of the star formation epoch and the lack of a difference between the two environments are not consistent with the predictions of standard semi-analytic models of galaxy formation (Kauffmann 1996, Kauffmann & Charlot 1998), where the stellar populations of the early-type galaxies in low-density environments (groups and clusters with velocity dispersions < 400 km s^{-1}) are predicted to have formed at $0.5 \lesssim z_f \lesssim 1.5$. Somerville & Primack (1998) have argued more generally that the earlier semi-analytic models (Kauffmann 1996, Kauffmann & Charlot 1998, Baugh et al. 1998) have systematically underestimated the typical star formation epoch through their choice of star formation mechanisms. Kauffmann & Charlot (1998) would argue, however, that early-type galaxies look old at all redshifts because the bulk of the star formation took place when the galaxies were morphologically late-type galaxies and that early-type galaxies are not assembled until the stellar populations look old. Such a bias is certainly present in the cluster samples, where many of the galaxies are morphologically selected, and galaxies with signs of recent star formation (E+A galaxies) are excluded from some of the samples (see van Dokkum & Franx 1996, Kelson et al. 1997, van Dokkum et al. 1998a, Pahre et al. 1999ab, Jorgensen et al. 1999). Such galaxies are a small fraction of their samples (10% overall, 20% in the highest redshift cluster), and so represent a modest bias. This argument also requires rapid number evolution in the early-type galaxy population by $z = 1$, for which there is little evidence in the field (e.g. Schade et al. 1999). Moreover, the lens systems were selected based on their mass, not their morphology. Studies of the effects of merging on gravitational lenses (Mao 1991, Mao & Kochanek 1994, Rix et al. 1994) concluded that the total number of lenses would be preserved but the balance would steadily shift to smaller image separations and late-type lenses at higher redshifts if there was rapid number evolution in the early-type galaxies. While we
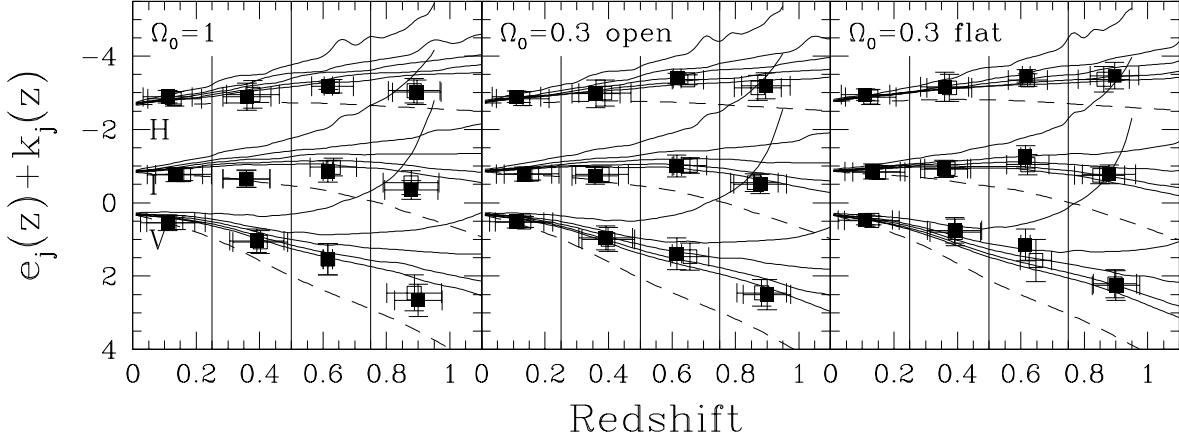
Fig. 8.— Evolution and K-corrections for the lens sample in the V=F555W, I=F814W and H=F160W bands as a function of redshift for the $\Omega_0 = 1$ (left), $\Omega_0 = 0.3$ open (middle) and $\Omega_0 = 0.3$ flat (right) cosmological models. The zero-redshift color differences were left in to separate the curves. The results are averages for all galaxies within the bins delineated by the vertical lines. The points are located at the mean redshift, and the redshift errorbar is the standard deviation of the redshift distribution in each bin. The error in the E+K correction is the standard deviation of the points, not the uncertainty in the mean (which would be smaller by $1/(N_{bin} - 1)^{1/2}$ where N_{bin} is the number of points in each bin). The filled points are the averages using only the lenses with known lens redshifts, while the open points include all lenses. The dashed curves are the no evolution models for each filter, and the solid curves are the instantaneous burst models with star formation redshifts (from bottom to top) of $z_f = 10, 3, 2, 1.5$ and 1.0 respectively.
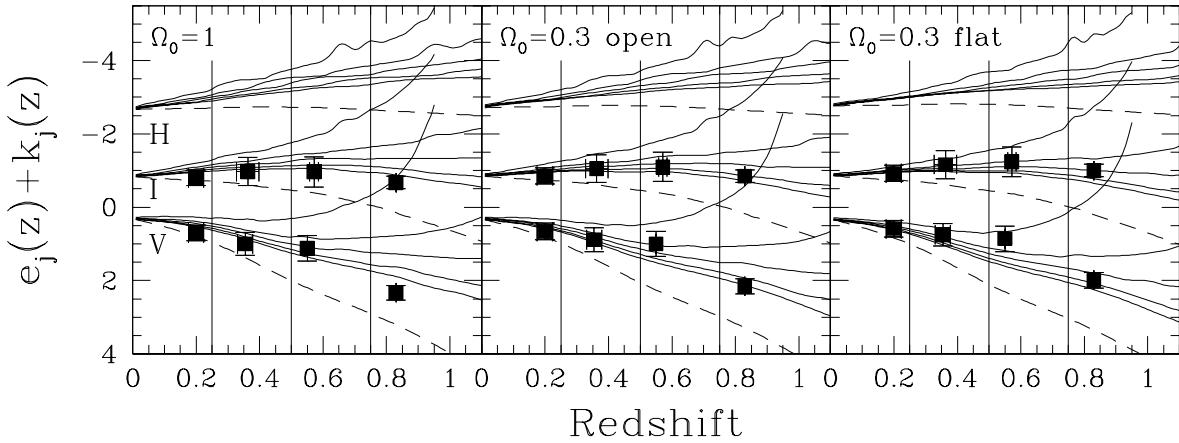

Fig. 9.— Evolution and K-corrections for the cluster sample in the V=F555W and I=F814W bands as a function of redshift for the $\Omega_0 = 1$ (left), $\Omega_0 = 0.3$ open (middle) and $\Omega_0 = 0.3$ flat (right) cosmological models. The format is identical to that of Figure 8.

omitted 11 lenses of the 41 for which we had obtained data, only 4 were dropped because they were clearly late-type lenses. In the absence of any population evolution we would have expected 4 to 8 late-type lenses in the sample. The others were dropped for the quality of the data or for possessing multiple lens galaxies. None of these systems have the blue, high surface brightness stellar populations which we would expect from the Kauffmann & Charlot (1998) scenario for how morphologically selected early-type galaxies could always appear to be old.

Missing lens redshifts are a major barrier to using the lenses as astrophysical and cosmological tools, so we also explored using photometric redshift estimates for the lens galaxies. Galaxy colors, particularly with the limited galaxy type range of the lenses, produce very good redshift estimates. The FP is also a good redshift estimator, but redshift estimates from the FP can have broad degeneracies when using infrared data for high redshift lens galaxies. Our redshift estimation method has an empirical accuracy of $\langle z_{FP} - z_l \rangle = -0.04 \pm 0.09$ for the 20 lenses with known redshifts. The scatter is dominated by lenses for which we possess only H-band data, and would be reduced by the inclusion of accurate infrared to optical color measurements. Small amounts of late-time star formation reduce the accuracy of our estimates, but lens galaxies with significant star formation or younger stellar populations will usually have easily measured spectroscopic redshifts.

In most systems we can only estimate the velocity dispersion of the lens galaxy from the geometry of the lensed images. Comparisons of these estimates both to the velocity dispersions predicted from the fundamental plane and direct measurements for four of the lenses indicated that a dark matter-dominated model is more consistent with the data than constant M/L models, and that a radially anisotropic constant M/L model was significantly better than an isotropic model. Our results for the normalization factor $f = \sigma_D/\sigma_c$ of the dark matter model are somewhat ambiguous, as we find $f \simeq 0.80 \pm 0.05$ if we match the three usable lens galaxy velocity dispersions and $f = 1.06 \pm 0.07$ if we match the zero-redshift mass-to-light ratios of the lens and cluster galaxies. The central surface brightnesses of the lens galaxies are similar to those of the cluster galaxies, so the velocity dispersions can usually measured if there are no nearby, bright source images. Five good candidates with surface brightnesses in a $1''0$ aperture above 23 R mag/arcsec^2 are MG1654+1346 ($\langle \mu_R \rangle = 20.2$), 0047–2808 ($\langle \mu_R \rangle = 21.1$), B0712+472 ($\langle \mu_R \rangle = 21.3$), B1608+656 ($\langle \mu_R \rangle = 21.7$), HST1411+5211 ($\langle \mu_R \rangle = 22.2$) and HST14176+5226 ($\langle \mu_R \rangle = 22.8$). The systems with measured velocity dispersions had central surface brightnesses of 17.7, 19.1, 20.2 and 21.1 R mag/arcsec^2 for Q 2237+0305, MG 1549+3047, Q 0957+561 and PG 1115+080 respectively. We would not have included Q 2237+0305, Q 0957+561 and PG 1115+080 in our list of dynamical targets because they also have bright quasar images which will contaminate the galaxy spectrum. With a larger number of directly measured dispersions, more sophisticated explorations of these dynamical issues would be possible.

REFERENCES

Baugh, C.M., Cole, S., Frenk, C.S., & Lacey, C.G., 1998, ApJ, 498, 504

Bernstein, G., Fischer, P., Tyson, J.A., & Rhee, G., 1997, ApJL, 483, 79

Binney, J.J. & Mamon, G.A., 1982, MNRAS, 200, 361

Bower, G.B., Lucey, J.R. & Ellis, R.S., 1992, 254, 601

Bruzual, A.G., & Charlot, S., 1993, ApJ, 405, 538

de Carvalho, R.R. & Djorgovski, S.G., 1992, ApJL, 389, L49

Djorgovski, S.G. & Davis, M., 1987, ApJ, 313, 59

Donahue, M., Voit, G.M., Gioia, I.M., Luppino, G., Hughes, J.P., & Stocke, J.T., 1998, ApJ, 502, 550

Dressler, A., Lynden-Bell, D., Burstein, D., Davies, R.L., Faber, S.M., Terlevich, R.J. & Wegner, G., 1987, ApJ, 313, 42

Dressler, A., Oemler, A., Sparks, B., Lucas, R.A., 1994, ApJL, 435, L23

Forbes, D.A., Ponman, T.J., & Brown, R.J.N., 1998, ApJ, 508, L43

Eisenhardt, P.R., Lee, L., Hogg, D.W., Soifer, B.T., Neugebauer, G., & Werner, M.W., 1996, ApJ, 461, 72

Ellis, R.S., Smail, I., Dressler, A., Couch, W.J., Oemler, A., Butcher, H. & Sharples, R.M., 1997, ApJ, 483, 582

Evans, A.S., Scoville, N.Z.,, Dinshaw, N., Armus, L., Soifer, B.T., Neugebauer, G., & Rieke, M., 1999, ApJ, 518, 145

Fabbiano, G. 1989, ARA&A, 27, 87

Faber, S.M. & Jackson, R.E., 1976, ApJ, 204, 668

Falco, E.E., Shapiro, I.I., Moustakas, L.A. & Davis, M., 1997, ApJ, 484, 70

Falco, E.E., Lehár, J., & Shapiro, I.I., 1997, AJ, 113, 540

Falco, E.E., Impey, C.D., Kochanek C.S., Lehár, J., McLeod, B.A., Rix, H.-W., Keeton, C.R., Muñoz, J.A., & Peng, C.Y., 1999, ApJ, 523, 617

Fassnacht, C.D., Blandford, R.D., Cohen, J.G., Matthews, K., Pearson, T.J., Readhead, A.C.S., Womble, D.S., Myers, S.T., Browne, I.W.A., Jackson, N.J., Marlow, D.R., Wlikinson, P.N., Koopmans, L.V.E., de Bruyn, A.G., Schilizzi, R.T., Bremer, M., Miley, G., 1999, AJ, 117, 658

Fischer, P., Schade, D., & Barientos, F., 1998, ApJL, 503, 127

Foltz, C.B., Hewett, P.C., Webster, R.L. & Lewis, G.F., 1992, ApJL, 386, 43L

Forbes, D.A., Ponman, T.J., & Brown, J.N., 1998, AJ, 508, L43

Fukugita, M., & Turner, E.L., 1991, MNRAS, 253, 99

Fukugita, M., Shimasaku, K. & Ichikawa, T., 1995, PASP, 107, 945

Guzman, R., & Lacey, J.R., 1993, MNRAS, 263, L47

Hernquist, L., 1990, ApJ, 356, 359

Helbig, P, & Kayser, R., 1996, A&A, 308, 359

Holtzman, J., et al, 1995, PASP, 107, 1065

Impey, C.D., Falco, E.E.,. Kochanek C.S., Lehár, J., McLeod, B.A., Rix, H.-W., Peng, C.Y., & Keeton, C.R., 1998, ApJ, 509, 551

Jackson, N., Helbig, P., Browne, I., Fassnacht, C.D., Koopmans, L., Marlow, D., & Wilkinson, P.N., 1998a, A&A, 334, L33

Jackson, N., Nair, S., Browne, I.W.A., Wilkinson, P.N., Muxlow, T.W.B., de Bruyn, A.G., Koopmans, L., Bremer, M., Snellen, I., Miley, G.K., Schilizzi, R.T., Myers, S., Fassnacht, C., Womble, D.S., Readhead, A.C.S., Blandford, R.D., Pearson, T.J., 1998b, MNRAS, 296, 483

James, P.A., & Mobasher, B., 1999, MNRAS, 306, 199

Jorgensen, I., 1999, MNRAS, 306, 607

Jorgensen, I. & Franx, M., 1994, ApJ, 433, 553

Jorgensen, I., Franx, M. & Kjaergaard, P., 1993, ApJ, 411, 34

Jorgensen, I., Franx, M. & Kjaergaard, P., 1995a, MNRAS, 273, 1097

Jorgensen, I., Franx, M. & Kjaergaard, P., 1995b, MNRAS, 276, 1341

Jorgensen, I., Franx, M. & Kjaergaard, P., 1996, MNRAS, 280, 167

Jorgensen, I., Franx, M., Hjorth, J., & van Dokkum, P.G., 1999, MNRAS, 308, 833

Kauffmann, G., 1996, MNRAS, 281, 487

Kauffmann, G., Charlot, S., & White, S.D.M., 1996, MNRAS, 283, 117L

Kauffmann, G. & Charlot, S., 1998, MNRAS, 294, 705

Keeton, C.R., Kochanek, C.S. & Falco, E.E., 1998, ApJ 509, 561

Kelson, D.D., van Dokkum, P.G., Franx, M. & Illingworth, G.D., 1997, ApJL, 478, L13

Kelson, D.D., Illingworth, G.D., van Dokkum, P.G., & Franx, M., 2000, ApJ, 531, 184

Kochanek, C.S., 1992, ApJ, 384, 1

Kochanek, C.S., 1993, ApJ, 419, 12

Kochanek, C.S., 1994, ApJ, 436, 56

Kochanek, C.S., 1995, ApJ, 445, 559

Kochanek, C.S., 1996, ApJ, 466, 638

Kochanek, C.S., Falco, E.E., Impey, C.D., Lehár, J., McLeod, B.A., Rix, H.-W., Keeton, C.R., Peng, C.Y., & Muñoz, J.A., 1998, astro-ph/9809371

Koopmans, L.V.E., de Bruyn, A.G., Marlow, D.R., Jackson, N., Blandford, R.D., Browne, I.W.A., Fassnacht, C.D., Myers, S.T., Pearson, T.J., Readhead, A.C.S., Wilkinson, P.N., Womble, D., 1999, MNRAS, 303, 727

Lehár, J., Falco, E.E., Impey, C.D., Kochanek, C.S., McLeod, B.A., Muñoz, J.A., Rix, H.-W., Keeton, C.R., & Peng, C.Y., 2000, ApJ, in press

Lehár, J., Cooke, A.J., Lawrence, C.R., Silber, A.D. & Langston, G.I., 1996, AJ, 111, 1812

Lilly, S.J., Treese, L., Hammer, F., Crampton, D., & Le Fevre, O.., 1995, ApJ, 455, 108L

Mao, S.D., 1991, ApJ, 380, 9

Mao, S.D., & Kochanek, C.S., 1994, MNRAS, 268, 569

Maoz, D., & Rix, H.-W.,. 1993, ApJ, 416, 425

Menten, K.M., Carilli, C.L., & Reid, M.J., 1999, Highly Redshifted Radio Lines, eds. Carilli, Radford, Menten, and Langston, (San Francisco: PASP), astro-ph/9812178

Myers, S.T., Fassnacht, C.D., Djorgovski, S.G., et al., 1995, ApJL, L5

Pahre, M.A., 1999, ApJ submitted

Pahre, M.A., de Carvalho, R.R. & Djorgovski, S.G., 1998a, AJ, 116, 1591

Pahre, M.A., de Carvalho, R.R. & Djorgovski, S.G., 1998b, AJ, 116, 1606

Pahre, M.A., Djorgovski, S.G., & de Carvalho, R.R. 1999a, ApJS submitted

Pahre, M.A., Djorgovski, S.G., & de Carvalho, R.R. 1999b, ApJL submitted

Ratnatunga, K.U., Ostrander, E.J., Griffiths, R.E., & Im, M., 1995, ApJL, 453, 5

Remy, M., Claeskens, J.-F., Surdej, J., Hjorth, J., Refsdal, S., Wucknitz, O., Sorensen, A.N., & Grundahl, F., 1998, NewA, 3, 379

Rhee, G., 1991, Nature, 350, 211

Rix, H.-W., de Zeeuw, P., Cretton, N., van der Marel, R.P. & Carollo, C.M. 1997, ApJ, 488, 702

Rix, H.-W., Maoz, D., Turner, E.L., & Fukugita, M., 1994, ApJ, 435, 49

Romanowsky, A.J., & Kochanek, C.S., 1999, ApJ, 516, 18

Schade, D., Carlberg, R.G., Yee, H.K.C., Lopez-Cruz, O. & Ellingson, E., 1996, ApJL, 464, L63

Schade, D., Lilly, S.J., Crampton, D., et al., 1999, ApJ, 525, 31

Schlegel, D.J., Finkbeiner, D.P., & Davis, M., 1998, ApJ, 500, 525

Smail, I., Dressler, A., Couch, W.J., Ellis, R.S., Oemler, A., Butcher, H., & Shaples, R.M., 1997, ApJS, 110, 213

Somerville, R.S., & Primack, J.R., 1998, astro-ph/9811001

Stanford, S.A., Eisenhardt, P.R. & Dickinson, M., 1998, 492, 461

Terlevich, A., Kuntschner, H., Bower, R.G., Caldwell, N., & Sharples, R.M., 1999, MNRAS, 310, 445

Tonry, J.L. 1998, AJ, 115, 1

Tonry, J.L. & Franx, M., 1999, ApJ, 515, 512

Trager, S.C., 1997, PhD thesis, University of California (Santa Cruz)

Treu, T., Stiavelli, M., Casertano, S., Moller, P., & Bertin, G., 1999, MNRAS, 308, 1037

Turner, E.L., Ostriker, J.P., & Gott, J.R., 1984, ApJ, 284, 1

van Dokkum, P.G. & Franx, 1996, MNRAS, 281, 985

van Dokkum, P.G., Franx, M., Kelson, D.D. & Illingworth, G.D., 1998a, ApJL, 504, L17

van Dokkum, P.G., Franx, M., Kelson, D.D. & Illingworth, G.D., Fisher, D. & Fabricant, D., 1998b, ApJ, 500, 714

van Dokkum, P.G., Franx, M., Fabricant, D., Kelson, D.D. & Illingworth, G.D., 1999, ApJL, 520, 95

Xanthopoulos, E., Browne, I.W.A., King, L.J., Koopmans, L.V.E., Jackson, N.J., Marlow, D.R., Patnaik, A.R., Porcas, R.W., Wilkinson, P.N., 1998, MNRAS, 300, 649

Zepf, S.E., 1997, Nature, 390, 377

Ziegler, B.L., Saglia, R.P., Bender, R., Belloni, P., Greggio, L., & Seitz, S., 1999, A&A, 346, 13

Table 1.   Summary of Lens Observations

Target	Camera/Filter	Time	Date	Source
0047-2808	WFPC2/F555W	9500	99.01.07	GO-6560, Warren
Q0142–100=UM673	NIC2/F160W	2560	97.08.15	Lehár et al. 2000
	WFPC2/F675W	2500	94.11.22	Keeton et al. 1998
	WFPC2/F555W	1200	94.11.22	Keeton et al. 1998
MG0414+0534	NIC2/F205W	640	97.08.14	CASTLES
	NIC2/F160W	10048	98.02.13	CASTLES
	NIC2/F110W	1792	97.08.14	CASTLES
	WFPC2/F814W	10500	94.11.08	Falco, Lehár & Shapiro 1997
	WFPC2/F675W	8100	94.11.08	Falco, Lehár & Shapiro 1997
B0712+472	NIC1/F160W	5248	97.08.24	Jackson et al. 1998a
	WFPC2/F814W	1000	96.01.29	Jackson et al. 1998b
	WFPC2/F555W	800	96.01.29	Jackson et al. 1998b
RXJ0911+0551	NIC2/F160W	2560	98.10.18	CASTLES
	WFPC2/F814W	1600	00.03.02	CASTLES
FBQ0951+2635	NIC2/F160W	2560	98.03.19	CASTLES
	WFPC2/F814W	1600	99.11.11	CASTLES
	WFPC2/F555W	1600	99.10.08	CASTLES
BRI0952–0115	NIC2/F160W	5120	97.10.17	Lehár et al. 2000
	WFPC2/F675W	5400	94.10.22	Keeton et al. 1998
Q0957+561	NIC2/F160W	2816	98.05.30	CASTLES
	WFPC2/F814W	2620	95.11.19	Bernstein et al. 1997
	WFPC2/F555W	32200	95.11.19	Bernstein et al. 1997
LBQS1009–0252	NIC2/F160W	2560	97.11.15	Lehár et al. 2000
	WFPC2/F814W	2600	99.01.01	Lehár et al. 2000
	WFPC2/F555W	1600	99.01.01	Lehár et al. 2000
Q1017–207=J03.13	NIC2/F160W	2560	97.11.14	Lehár et al. 2000
	WFPC2/F814W	2300	95.11.28	GO-5958, Surdej
FSC10214+472	NIC2/F205W	384	97.10.27	Evans et al. 1999
	NIC2/F110W	384	97.10.27	Evans et al. 1999
	WFPC2/F814W	6600	94.12.10	Eisenhardt et al. 1996
B1030+071	NIC1/F160W	2624	97.11.20	Lehár et al. 2000
	WFPC2/F814W	1000	97.02.03	Xanthopoulos et al. 1998
	WFPC2/F555W	1000	97.02.03	Xanthopoulos et al. 1998

Table 1—Continued

Target	Camera/Filter	Time	Date	Source
HE1104–1805	NIC2/F160W	2560	97.11.22	Lehár et al. 2000
	WFPC2/F814W	1000	95.11.19	Remy et al. 1998
	WFPC2/F555W	1600	00.02.04	CASTLES
PG1115+080	NIC2/F160W	2560	97.11.17	Impey et al. 1998
	WFPC2/F814W	4400	97.05.17	GO-6555, Schechter
	WFPC2/F555W	3200	99.03.31	CASTLES
B1127+385	NIC1/F160W	2624	98.04.10	GO-7873, Wilkinson
	WFPC2/F814W	1000	96.06.21	Koopmans et al. 1999
MG1131+0456	NIC2/F160W	5120	98.01.05	Kochanek et al. 1999
	WFPC2/F814W	10500	95.04.18	Kochanek et al. 1999
	WFPC2/F675W	8100	95.04.18	Kochanek et al. 1999
HST12531–921	NIC2/F160W	5120	98.02.14	CASTLES
	WFPC2/F814W	8400	95.02.15	Ratnatunga et al. 1995
	WFPC2/F606W	5400	95.02.15	Ratnatunga et al. 1995
HST14113+521	WFPC2/F702W	12600	94.07.25	Fischer, Schade & Barientos, 1998
HST14176+522	NIC2/F160W	5632	98.05.28	CASTLES
	WFPC2/F814W	4400	94.03.11	Ratnatunga et al. 1995
	WFPC2/F606W	2800	94.03.11	Ratnatunga et al. 1995
B1422+231	NIC2/F160W	5120	98.02.27	CASTLES
	WFPC2/F791W	4200	99.02.06	GO-6652, Impey
	WFPC2/F555W	4200	99.02.06	GO-6652, Impey
SBS1520+530	NIC2/F160W	2816	98.07.20	CASTLES
	WFPC2/F814W	1600	99.11.09	CASTLES
MG1549+3047	NIC2/F205W	704	97.08.17	CASTLES
	NIC2/F160W	1536	97.08.17	CASTLES
	WFPC2/F814W	560	99.05.20	CASTLES
	WFPC2/F555W	560	99.05.20	CASTLES
B1608+656	NIC2/F160W	2816	97.09.29	CASTLES
	WFPC2/F814W	2400	96.04.07	Jackson et al. 1998a
	WFPC2/F555W	1500	96.04.07	Jackson et al. 1998a

Table 1—Continued

Target	Camera/Filter	Time	Date	Source
MG1654+1346	NIC2/F160W	2560	97.10.12	CASTLES
	WFPC2/F814W	10500	96.01.19	Keeton, Kochanek & Falco 1998
	WFPC2/F675W	5826	96.01.18	Keeton, Kochanek & Falco 1998
B1938+666	NIC2/F160W	5632	97.10.07	CASTLES
	WFPC2/F814W	3000	99.04.24	CASTLES
	WFPC2/F555W	2800	99.04.24	CASTLES
MG2016+112	NIC2/F160W	5120	97.10.30	CASTLES
	WFPC2/F814W	2600	99.05.14	GO-6543, Lawrence
	WFPC2/F555W	2600	99.05.14	GO-6543, Lawrence
B2045+265	NIC1/F160W	2624	97.07.14	Fassnacht et al. 1999
HE2149–2745	NIC2/F160W	2560	98.09.04	CASTLES
	WFPC2/F814W	1600	99.10.24	CASTLES
Q2237+030	NIC2/F205W	704	97.10.11	CASTLES
	NIC2/F160W	1532	97.10.11	CASTLES
	WFPC2/F814W	120	99.10.20	CASTLES
	WFPC2/F555W	1600	95.06.23	GO-5236, Westphal
B2319+052	NIC1/F160W	2624	98.05.30	GO-7873, Wilkinson

Note. — The exposure time is in seconds. The Source entry is either the first published discussion of the data or the HST program ID and PI for unpublished data.

Table 2.   Summary of Cluster Observations

Cluster	z_c	E_{Gal}	#	Filter	Time	Date	Source
A665	0.18	0.045	1	F814W	4800	94.12.02	GO-5458, Franx
			1	F606W	5100	94.12.02	GO-5458, Franx
			2	F814W	4400	94.10.31	GO-5458, Franx
			2	F606W	4400	94.10.31	GO-5458, Franx
A2390	0.23	0.113	1	F814W	10500	94.12.10	GO-5352, Fort
			1	F555W	8400	94.12.10	GO-5352, Fort
CL1358+62	0.33	0.024	1	F814W	3600	96.02.12	Kelson et al. 1997
			1	F606W	3600	96.02.12	Kelson et al. 1997
A370	0.37	0.032	1	F675W	5600	95.12.02	Ziegler et al. 1999
			2	F814W	12600	95.01.12	Smail et al. 1997
			2	F555W	8000	95.01.12	Smail et al. 1997
A851	0.41	0.015	1	F702W	4400	97.04.23	GO-6480, Dressler
			2	F702W	21000	94.01.10	Dressler et al. 1994
			3	F814W	12600	94.04.18	Smail et al. 1997
			3	F555W	8000	94.04.18	Smail et al. 1997
MS0015+16	0.55	0.056	1	F814W	16800	94.12.11	Smail et al. 1997
			1	F555W	12600	94.12.11	Smail et al. 1997
MS2053–04	0.58	0.084	1	F814W	2100	97.12.13	Kelson et al. 1997
			1	F702W	2400	95.10.23	Kelson et al. 1997
			2	F814W	1100	97.12.11	Kelson et al. 1997
			3	F814W	2100	97.12.13	Kelson et al. 1997
MS1054–03	0.83	0.024	1	F814W	15600	96.03.13	Donahue et al. 1998
			1	F606W	6500	98.05.26	van Dokkum et al. 1999

Note. — The "#" entry is an arbitrary number to indicate which images overlap. The exposure time is in seconds. $E_{Gal} = E(B - V)$ is the foreground Galactic extinction from Schlegel, Finkbeiner & Davis (1998). The source of the photometry is either the first published paper discussing the observations or the program identification.

Table 3.   Lens Galaxy Photometric Data

Lens	E_{Gal} (mag)	$\Delta\theta$ $('')$	$\log(r_e/'')$	μ_e (mag/asec^2)	σ_{FP}	Filter 1	color (mag)	Filter 2
0047-2808	0.016	2.70	-0.04 ± 0.02	22.45 ± 0.08	0.01	F555W		
Q0142-100	0.031	2.24	-0.29 ± 0.02	17.17 ± 0.09	0.03	F160W	4.18 ± 0.02	F555W
							2.72 ± 0.01	F675W
MG0414+0534	0.303	2.38	-0.11 ± 0.08	18.98 ± 0.23	0.02	F160W	1.67 ± 0.03	F110W
							0.84 ± 0.12	F205W
							5.04 ± 0.13	F675W
							3.37 ± 0.05	F814W
B0712+472	0.113	1.42	-0.44 ± 0.06	16.95 ± 0.14	0.05	F160W	4.47 ± 0.06	F555W
							2.34 ± 0.07	F814W
RXJ0911+0551	0.045	2.21	-0.17 ± 0.04	19.10 ± 0.14	0.02	F160W	2.54 ± 0.09	F814W
FBQ0951+2635	0.022	1.11	-0.78 ± 0.10	15.96 ± 0.32	0.07	F160W	3.16 ± 0.04	F555W
							1.81 ± 0.03	F814W
BRI0952-0115	0.063	1.00	-1.00 ± 0.12	15.97 ± 0.45	0.09	F160W	3.13 ± 0.03	F675W
Q0957+561	0.009	6.26	0.30 ± 0.04	18.63 ± 0.11	0.03	F160W	3.91 ± 0.06	F555W
							1.98 ± 0.03	F814W
LBQS1009-025	0.034	1.54	-0.71 ± 0.08	17.69 ± 0.28	0.05	F160W	5.46 ± 0.22	F555W
							2.63 ± 0.04	F814W
Q1017-207	0.046	0.85	-0.52 ± 0.02	18.64 ± 0.06	0.06	F160W	2.56 ± 0.48	F814W
FSC10214+472	0.012	1.59	0.05 ± 0.05	22.67 ± 0.12	0.03	F814W	1.11 ± 0.36	F110W
							3.36 ± 0.41	F205W
B1030+071	0.022	1.56	-0.37 ± 0.03	20.32 ± 0.09	0.01	F814W	2.51 ± 0.21	F160W
							2.56 ± 0.04	F555W
HE1104-1805	0.056	3.19	-0.19 ± 0.13	18.49 ± 0.38	0.03	F160W	5.67 ± 0.50	F555W
							2.54 ± 0.10	F814W
PG1115+080	0.041	2.29	-0.33 ± 0.02	17.00 ± 0.08	0.02	F160W	4.08 ± 0.04	F555W
							2.26 ± 0.02	F814W
B1127+385	0.027	0.70	-1.01 ± 0.21	16.97 ± 0.56	0.07	F160W	2.68 ± 0.56	F814W
MG1131+0456	0.036	2.10	-0.24 ± 0.05	19.42 ± 0.17	0.04	F160W	3.85 ± 0.06	F675W
							2.59 ± 0.04	F814W

Table 3—Continued

Lens	E_{Gal} (mag)	$\Delta\theta$ ($''$)	$\log(r_e/'')$	μ_e (mag/asec^2)	σ_{FP}	Filter 1	color (mag)	Filter 2
HST12531-291	0.079	1.09	-0.85 ± 0.03	17.22 ± 0.11	0.04	F160W	4.33 ± 0.03	F606W
							2.33 ± 0.03	F814W
HST14113+521	0.016	1.72	-0.32 ± 0.05	20.87 ± 0.17	0.04	F702W		
HST14176+522	0.007	2.84	-0.15 ± 0.05	18.76 ± 0.14	0.03	F160W	4.36 ± 0.08	F606W
							2.20 ± 0.09	F814W
B1422+231	0.048	1.56	-0.50 ± 0.13	17.07 ± 0.45	0.06	F160W	4.23 ± 0.05	F555W
							2.09 ± 0.06	F791W
SBS1520+530	0.016	1.59	-0.46 ± 0.04	17.52 ± 0.12	0.02	F160W	2.32 ± 0.13	F814W
MG1549+3047	0.029	1.70	-0.06 ± 0.02	16.39 ± 0.04	0.02	F160W	0.68 ± 0.01	F205W
							3.51 ± 0.02	F555W
							2.02 ± 0.02	F814W
B1608+656	0.031	2.27	-0.19 ± 0.07	17.78 ± 0.23	0.02	F160W	4.48 ± 0.23	F555W
							2.18 ± 0.35	F814W
MG1654+1346	0.061	2.10	-0.05 ± 0.02	17.57 ± 0.04	0.02	F160W	2.72 ± 0.01	F675W
							2.07 ± 0.02	F814W
B1938+666	0.121	1.00	-0.16 ± 0.04	19.86 ± 0.12	0.04	F160W	5.78 ± 0.84	F555W
							2.79 ± 0.08	F814W
MG2016+112	0.235	3.26	-0.68 ± 0.03	17.05 ± 0.12	0.04	F160W	7.39 ± 0.08	F555W
							3.47 ± 0.01	F814W
B2045+265	0.235	2.28	-0.42 ± 0.13	18.14 ± 0.44	0.09	F160W		
HE2149-2745	0.072	1.70	-0.30 ± 0.02	18.10 ± 0.05	0.05	F160W	1.95 ± 0.03	F814W
Q2237+030	0.071	1.76	0.55 ± 0.11	17.06 ± 0.29	0.07	F160W	0.44 ± 0.26	F205W
							3.29 ± 0.28	F555W
							2.44 ± 0.01	F675W
							2.26 ± 0.01	F814W
B2319+052	0.064	1.36	-0.65 ± 0.02	16.92 ± 0.05	0.03	F160W		

Note. — For each lens, $E_{Gal} = E(B - V)$ is the foreground Galactic extinction from Schlegel, Finkbeiner & Davis (1998) and $\Delta\theta$ is the image separation. For the reference filter (Filter 1) we present values and uncertainties for the logarithm of the intermediate axis effective radius, $\log(r_e/'')$, the mean surface brightness inside the effective radius, μ_e, and the uncertainty σ_{FP} for the variable combination $\mu_e - 3.03 \log(r_e)$ appearing in the fundamental plane equations (see eqn. (2)). We then provide the colors measured between Filter 1 and Filter 2 (blue minus red), with one color per line of the table. The magnitudes and colors are *not* corrected for the foreground extinction, but an $R_V = 3.1$ extinction curve is used to correct the magnitudes in all calculations and figures.

Table 4.   Cluster Galaxy Photometric Data

Cluster	Galaxy	$\log(\sigma_c/\mathrm{km\ s}^{-1})$	$\log(r_e/'')$	μ_e (mag/asec^2)	Filter 1	color (mag)	Filter 2
A665	3	2.439 ± 0.013	0.34	19.78	F814W	1.05 ± 0.05	F606W
	15	2.414 ± 0.021	0.18	19.70	F814W	1.05 ± 0.05	F606W
	26	2.355 ± 0.024	0.03	19.28	F814W	1.02 ± 0.05	F606W
	42	2.395 ± 0.018	0.02	19.21	F814W	1.11 ± 0.05	F606W
	57	2.325 ± 0.021	-0.18	18.73	F814W	1.01 ± 0.05	F606W
	61	2.358 ± 0.012	-0.15	18.93	F814W	1.13 ± 0.05	F606W
	77	2.173 ± 0.030	0.11	20.39	F814W	1.06 ± 0.05	F606W
	80	2.276 ± 0.028	-0.18	19.12	F814W	0.99 ± 0.05	F606W
A2390	6	2.313 ± 0.017	0.01	19.67	F814W	1.65 ± 0.05	F555W
	7	2.277 ± 0.019	0.17	20.16	F814W	1.68 ± 0.05	F555W
	9	2.371 ± 0.011	-0.21	18.63	F814W	1.64 ± 0.05	F555W
	10	2.250 ± 0.020	-0.22	19.33	F814W	1.76 ± 0.05	F555W
	138	2.029 ± 0.017	-0.13	20.87	F814W	1.66 ± 0.05	F555W
CL1358	236	2.220 ± 0.029	-0.24	19.69	F814W	1.26 ± 0.05	F606W
	256	2.436 ± 0.011	-0.01	19.43	F814W	1.17 ± 0.05	F606W
	269	2.534 ± 0.013	-0.08	19.27	F814W	1.28 ± 0.05	F606W
	298	2.447 ± 0.012	-0.13	19.31	F814W	1.21 ± 0.05	F606W
	375	2.479 ± 0.016	0.39	20.96	F814W	1.27 ± 0.05	F606W
	408	2.423 ± 0.028	-0.40	19.02	F814W	1.17 ± 0.05	F606W
	454	2.233 ± 0.015	0.19	21.08	F814W	1.22 ± 0.05	F606W
	470	2.267 ± 0.014	-0.04	19.91	F814W	1.15 ± 0.05	F606W
A370	1	2.519 ± 0.005	0.33	21.51	F675W		
	2	2.404 ± 0.007	0.95	23.42	F675W		
	10	2.291 ± 0.009	0.15	21.66	F675W		
	24	2.399 ± 0.007	-0.10	20.51	F675W		
	28	2.345 ± 0.008	-0.17	19.92	F814W	1.90 ± 0.05	F555W
	41	2.467 ± 0.009	-0.29	19.39	F814W	2.07 ± 0.05	F555W
	67	2.207 ± 0.011	0.01	21.05	F814W	1.96 ± 0.05	F555W
	77	1.976 ± 0.019	-0.04	21.71	F675W		
	79	2.227 ± 0.011	-0.34	20.28	F675W		
A851	23	2.273 ± 0.019	-0.19	20.31	F702W		
	57	2.299 ± 0.018	-0.39	19.91	F702W		
	69	2.288 ± 0.014	-0.24	20.43	F814W	1.86 ± 0.05	F555W
	102	2.173 ± 0.018	-0.63	19.78	F702W		
	111	1.766 ± 0.031	-0.26	21.36	F702W		

Table 4—Continued

Cluster	Galaxy	$\log(\sigma_c/\mathrm{km\ s^{-1}})$	$\log(r_e/'')$	μ_e (mag/asec^2)	Filter 1	color (mag)	Filter 2
MS0015	2	2.412 ± 0.018	1.01	23.84	F814W	2.48 ± 0.05	F555W
	7	2.291 ± 0.009	-0.29	19.97	F814W	2.59 ± 0.05	F555W
	13	2.422 ± 0.017	-0.39	19.69	F814W	2.40 ± 0.05	F555W
	56	2.337 ± 0.017	-1.50	15.68	F814W	2.48 ± 0.05	F555W
MS2053	197	2.504 ± 0.025	0.20	21.59	F814W	0.83 ± 0.05	F702W
	311	2.348 ± 0.049	-0.42	20.45	F814W	0.78 ± 0.05	F702W
	422	2.120 ± 0.060	-0.51	20.05	F814W	0.74 ± 0.05	F702W
	432	2.207 ± 0.054	-0.30	20.96	F814W	0.73 ± 0.05	F702W
	551	2.336 ± 0.038	-0.66	19.56	F814W	0.79 ± 0.05	F702W
MS1054	1294	2.500 ± 0.029	-0.18	21.35	F814W	2.18 ± 0.05	F606W
	1359	2.352 ± 0.037	-0.52	20.39	F814W	2.43 ± 0.05	F606W
	1405	2.413 ± 0.035	-0.02	21.87	F814W	2.25 ± 0.05	F606W
	1457	2.322 ± 0.050	-0.24	21.42	F814W	2.10 ± 0.05	F606W
	1484	2.519 ± 0.026	0.19	22.24	F814W	2.43 ± 0.05	F606W
	1567	2.417 ± 0.045	-0.33	21.09	F814W	2.17 ± 0.05	F606W

Note. — The variables are the same as in Table 3 except for the velocity dispersion σ_c replacing the image separation $\Delta\theta$. The velocity dispersions for A665, A2390, A370, A851 and MS0015+16 are from Pahre et al. (1999a), those for CL1358+62 and MS2053–04 are from Kelson et al. (1997), and those for MS1054–03 are from van Dokkum et al. (1998).

Table 5.   Lens Galaxy Redshift Estimates

Lens	z_l	z_s	z_{FP}	z_{min}	z_{max}	N_{filt}
0047-2808	0.48	3.60	0.39	0.35	0.48	1
Q0142-100	0.49	2.72	0.36	0.33	0.38	3
MG0414+0534	0.96	2.64	0.89	0.76	0.94	5
B0712+472	0.41	1.34	0.33	0.31	0.35	3
RXJ0911+0551	0.77	2.80	0.82	0.74	0.92	2
FBQ0951+2635		1.24	0.21	0.18	0.23	3
BRI0952-0115		4.50	0.41	0.36	0.46	2
Q0957+561	0.36	1.41	0.37	0.34	0.39	3
LBQS1009-025		2.74	0.88	0.77	0.92	3
Q1017-207		2.55	0.78	0.73	0.87	2
FSC10214+472		2.29	0.78	0.68	0.81	3
B1030+071	0.60	1.54	0.54	0.51	0.68	3
HE1104-1805		2.32	0.73	0.69	0.76	3
PG1115+080	0.31	1.72	0.29	0.27	0.35	3
B1127+385			0.78	0.62	1.03	2
MG1131+0456	0.84		0.95	0.86	1.01	3
HST12531-291			0.63	0.60	0.83	3
HST14113+521	0.46	2.81	0.51	0.44	0.57	1
HST14176+522	0.81	3.40	0.71	0.66	0.79	3
B1422+231	0.34	3.62	0.37	0.35	0.39	3
SBS1520+530		1.86	0.52	0.44	0.65	2
MG1549+3047	0.11		0.12	0.10	0.14	4
B1608+656	0.63	1.39	0.45	0.43	0.48	3
MG1654+1346	0.25	1.74	0.25	0.22	0.29	3
B1938+666	0.88		0.84	0.81	1.04	3
MG2016+112	1.01	3.27	0.99	0.96	1.01	3
B2045+265	0.87	1.28	0.68	0.56	0.76	1
HE2149-2745		2.03	0.43	0.37	0.50	2
Q2237+030	0.04	1.69	0.02	0.02	0.03	5
B2319+052	0.62		0.61	0.27	0.88	1

Note. — N_{filt} is the number of filters available for the measurement. All examples with $N_{filt} = 1$ except HST14113+521 are H band observations. The redshift uncertainties are the formal uncertainties defined by the region where $\Delta\chi^2 < 4$. The actual accuracy is better characterized by the scatter observed in Figure 5.

Table 6.   E+K Corrections

Data	Band	N	$\langle z \rangle$	$\Omega_0 = 1$ Flat $\langle e + k \rangle$	$\Omega_0 = 0.3$ Open $\langle e + k \rangle$	$\Omega_0 = 0.3$ Flat $\langle e + k \rangle$
Lens 1	V	4	0.11 ± 0.09	0.21 ± 0.12	0.19 ± 0.10	0.13 ± 0.08
		8	0.39 ± 0.09	0.71 ± 0.12	0.62 ± 0.12	0.41 ± 0.13
		2	0.62 ± 0.01	1.21 ± 0.43	1.06 ± 0.44	0.80 ± 0.44
		5	0.90 ± 0.07	2.34 ± 0.22	2.16 ± 0.21	1.91 ± 0.20
	I	3	0.13 ± 0.09	0.08 ± 0.13	0.07 ± 0.13	0.01 ± 0.15
		5	0.36 ± 0.07	0.19 ± 0.12	0.12 ± 0.11	-0.06 ± 0.12
		2	0.62 ± 0.01	-0.01 ± 0.30	-0.14 ± 0.30	-0.39 ± 0.30
		6	0.88 ± 0.08	0.49 ± 0.11	0.35 ± 0.12	0.09 ± 0.12
	H	5	0.11 ± 0.08	-0.20 ± 0.09	-0.15 ± 0.08	-0.18 ± 0.08
		6	0.36 ± 0.08	-0.20 ± 0.17	-0.23 ± 0.17	-0.39 ± 0.18
		3	0.62 ± 0.01	-0.50 ± 0.07	-0.65 ± 0.10	-0.69 ± 0.12
		9	0.90 ± 0.08	-0.32 ± 0.12	-0.45 ± 0.13	-0.69 ± 0.13
Lens 2	V	5	0.14 ± 0.09	0.21 ± 0.09	0.19 ± 0.07	0.14 ± 0.06
		9	0.40 ± 0.09	0.74 ± 0.11	0.67 ± 0.12	0.46 ± 0.13
		2	0.62 ± 0.01	1.21 ± 0.43	1.14 ± 0.26	1.23 ± 0.33
		8	0.89 ± 0.09	2.13 ± 0.19	2.12 ± 0.15	1.86 ± 0.17
	I	4	0.16 ± 0.09	0.07 ± 0.10	0.07 ± 0.09	0.03 ± 0.11
		5	0.36 ± 0.07	0.19 ± 0.12	0.08 ± 0.10	-0.07 ± 0.09
		4	0.63 ± 0.07	-0.13 ± 0.14	-0.16 ± 0.13	-0.18 ± 0.14
		13	0.88 ± 0.09	0.30 ± 0.10	0.31 ± 0.08	0.11 ± 0.08
	H	6	0.13 ± 0.09	-0.14 ± 0.09	-0.10 ± 0.08	-0.11 ± 0.09
		7	0.38 ± 0.08	-0.26 ± 0.15	-0.25 ± 0.13	-0.36 ± 0.14
		5	0.63 ± 0.07	-0.49 ± 0.09	-0.61 ± 0.07	-0.58 ± 0.07
		17	0.89 ± 0.08	-0.36 ± 0.08	-0.40 ± 0.09	-0.60 ± 0.10
Cluster	V	13	0.20 ± 0.02	0.37 ± 0.06	0.33 ± 0.07	0.25 ± 0.07
		18	0.35 ± 0.02	0.67 ± 0.08	0.55 ± 0.08	0.41 ± 0.07
		4	0.55 ± 0.00	0.79 ± 0.20	0.66 ± 0.20	0.52 ± 0.20
		6	0.83 ± 0.00	2.01 ± 0.09	1.83 ± 0.09	1.65 ± 0.10
	I	13	0.20 ± 0.02	0.04 ± 0.06	0.01 ± 0.06	-0.06 ± 0.06
		16	0.36 ± 0.04	-0.13 ± 0.10	-0.19 ± 0.10	-0.30 ± 0.10
		14	0.57 ± 0.01	-0.12 ± 0.11	-0.24 ± 0.11	-0.37 ± 0.11
		6	0.83 ± 0.00	0.17 ± 0.08	0.01 ± 0.07	-0.14 ± 0.08

Note. — The "Lens 1" data include only lenses with known redshifts, while the "Lens 2" data include all systems using the redshift estimates of §4. The E+K corrections are computed in redshift bins with edges at $z = 0.25$, 0.50 and 0.75. For each bin, $\langle z \rangle$ gives the mean and dispersion of the redshifts for the N estimates in the bin. The uncertainty in the E+K correction is simply the dispersion of the values in the bin divided by $(N - 1)^{1/2}$.